Molecular Dynamics simulations of magnetron (reactive) sputtering and deposition

Pascal Brault
GREMI UMR7344 CNRS – Université d'Orléans
14, rue d'Issoudun BP6744
45067 ORLEANS Cedex 2, France

pascal.brault@univ-orleans.fr

All what should be known is here ☺

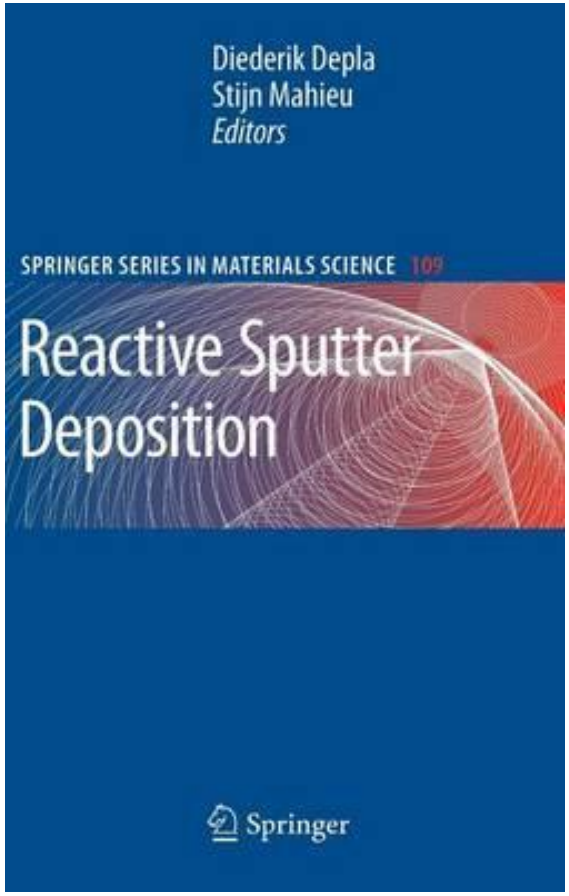

nevertheless …

Outline

- ✓ (Reactive) Magnetron sputtering as an atom (molecule, cluster) source
- ✓ Molecular Dynamics principles
- ✓ Molecular Dynamics of sputtering
- ✓ Molecular Dynamics of reactive sputtering
- ✓ Molecular Dynamics of deposition
- ✓ Conclusions/Perspectives

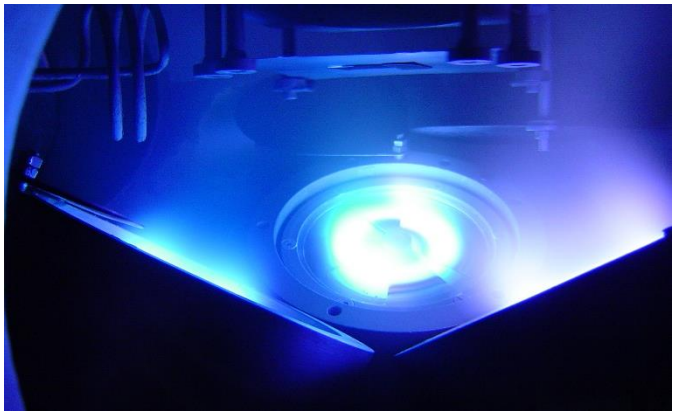

Plasma sputtering: A controled atom source

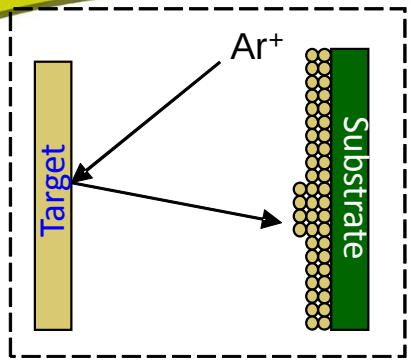

atom sources:

vapor at T_g (gas or evaporation : MB dist. of velocities),
Molecular beams ($E_k \approx$ 0.01 – 10 eV + T_g)
Sputtering (plasma, ion beam)
→ Thompson distribution of sputtered atoms

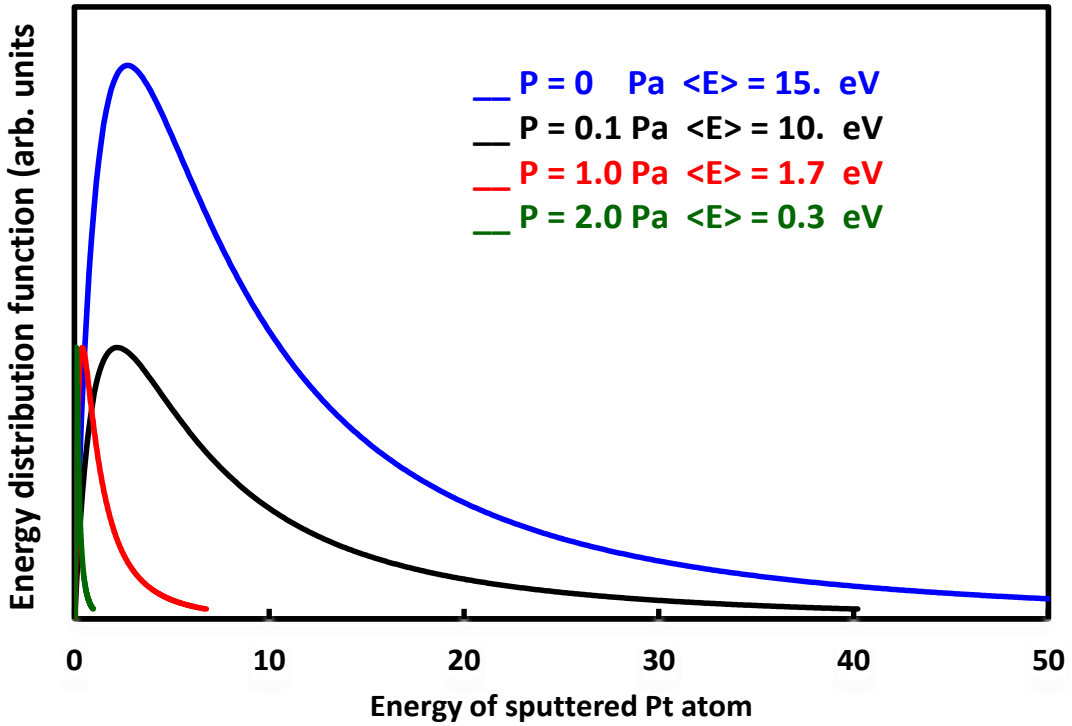

Sputtered Pt atom energy distribution
Target – substrate distance = 10 cm, Bias 300 V

$$f(E) \propto \frac{1-\left(\frac{E_{coh}+E}{\Lambda E_{Ar^+}}\right)^{\frac{1}{2}}}{E^2\left(1+\frac{E_{coh}}{E}\right)^3}$$

$$E_F = \left(E - k_B T_g\right)\exp\left[n \ln\left(E_f / E_i\right)\right] + k_B T_g$$

$$n = \frac{d_{T-S} P \sigma}{k_B T_g}$$

Pressure effect on energy distribution:
P ↗ f(E) → MB, ∀ f(E) and then <E> ↘

Pressure P
Bias V_b, Discharge current
Target to substrate distance

ϕ_{Ar+}
E_{Ar+}
reactive species

ϕ_{Ar+}
E_{Ar+}
$\phi_{sputt.\ mat}$
$\theta_{sputt.\ mat}$
$E_{sputt.\ mat}$

Sputtering

Ion flux : 1 A = 6.25 10^{18} s^{-1}
4'' target => $\phi_{ion} \approx 10^{17}$ cm^{-2} s^{-1}
sputtering rate $\gamma(V_b) \approx 0.01 - 3$

Sputtered atom deposition

$\phi_{atom} \approx 10^{15}$at $cm^{-2}s^{-1}$
Sticking coefficient : 0.01 - 1
condensation

Sputtering step

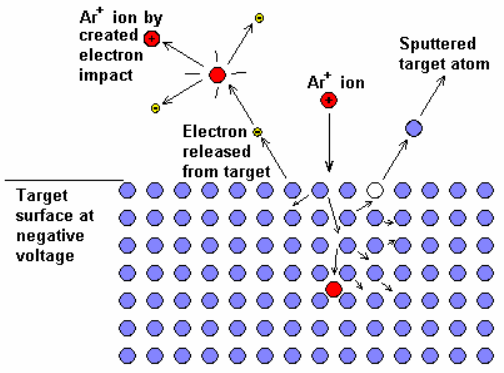

Deposition step

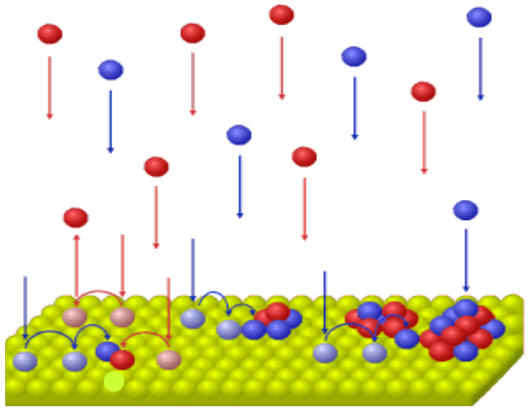

sputtering and deposition
⇒ atomic scale processes
⇒ MD is suitable

Molecular Dynamics:
Solving equations of motion :

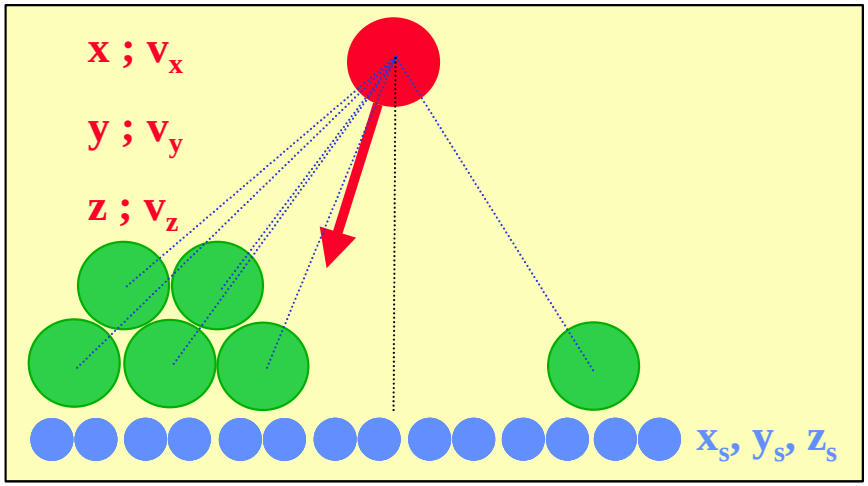

$$m_j \frac{\partial^2}{\partial t^2} x_j = -\frac{\partial}{\partial x_j} V_s - \sum_{i \neq j} \frac{\partial}{\partial x_j} V_{ij}$$

$$m_j \frac{\partial^2}{\partial t^2} y_j = -\frac{\partial}{\partial y_j} V_s - \sum_{i \neq j} \frac{\partial}{\partial y_j} V_{ij}$$

$$m_j \frac{\partial^2}{\partial t^2} z_j = -\frac{\partial}{\partial z_j} V_s - \sum_{i \neq j} \frac{\partial}{\partial z_j} V_{ij}$$

Velocity Verlet algorithm: universally stable.

$$v(t + \frac{1}{2}\Delta t) = v(t) + \frac{1}{2} a(t)\Delta t$$

$$r(t + \Delta t) = r(t) + v(t + \frac{1}{2}\Delta t)\Delta t$$

Force calculation a(t+Δt)

$$v(t + \Delta t) = v(t + \frac{1}{2}\Delta t) + \frac{1}{2} a(t + \Delta t)\Delta t$$

All the trajectories and deduced (statistical) quantities are depending on the interaction potentials:

- DFT and ab-initio initial parametrization

- Semi-empirical model → ad-hoc functions parametrized on macroscopic properties: lattice parameter, cohesive energy, surface energy, angles, elastic constants, bonds, …

D. B. Graves & P. Brault, Molecular dynamics for low temperature plasma-surface interaction studies, J. Phys. D 42 (2009) 194011
S. Erkoc, Empirical potential energy functions used in the simulations of materials properties, Annual Reviews of Computational Physics IX (2001) 1-103

Additive pairwise interactions:

Lennard-Jones potential

$$U_{ij} = 4\epsilon\left[\left(\frac{\sigma}{r_{ij}}\right)^{12} - \left(\frac{\sigma}{r_{ij}}\right)^{6}\right]$$

Morse potential

$$U_{ij} = D[e^{-2\alpha(r_{ij}-r_0)} - 2e^{-\alpha(r_{ij}-r_0)}]$$

Buckingham potential

$$V_{ij}(r_{ij}) = A\exp\left(-\frac{r_{ij}}{r_B}\right) - \frac{C_6}{r_{ij}^6}$$

Molière potential

$$V_M(r_{ij}) = \frac{Z_1 Z_2 e^2}{4\pi\varepsilon_0 r_{ij}}\sum_{i=1}^{3} c_i \exp\left(-d_i\frac{r_{ij}}{a_F}\right)$$

and ZBL potential
(rare gas – surface
and short range part)

$$V_{ZBL}(r_{ij}) = \frac{Z_1 Z_2 e^2}{4\pi\varepsilon_0 r_{ij}}\sum_{i=1}^{4} c_i \exp\left(-d_i\frac{r_{ij}}{a_U}\right)$$

$$a_F = \frac{0.83\left(\frac{9\pi^2}{128}\right)^{1/3} a_B}{\left(Z_1^{1/2} + Z_2^{1/2}\right)^{2/3}} \quad \text{and} \quad a_U = \frac{0.8853 a_B}{\left(Z_1^{0.23} + Z_2^{0.23}\right)}$$

with $a_B = 0.529\,177$ Å

Molecular Dynamics Simulations Potentials

	Morse potential			L-J potential		Buckingham potential		
Species	D_0 (eV)	α (Å^{-1})	r_0 (Å)	ε (Å)	σ (eV)	A (eV)	r_B (Å)	C_6 (eV Å^6)
Ag	0.3294	1.3939	3.096					
Al				0.392	2.62	5131.179	0.3224	248.0
Ar			—	0.01	3.4			
Au	0.4826	1.6166	3.004	0.449	2.637			
Ba	0.1416	0.656 98	5.373					
C				3.4	2.41×10^{-3}			
Ca	0.1623	0.805 35	4.569	0.215	3.6			
Cr	0.4414	1.5721	2.754	0.502	2.336			
Cs	0.044 85	0.415 69	7.557					
Cu	0.3446	1.3921	2.864	0.409	2.338			
Fe	0.4216	1.3765	2.849	0.527	2.321			
Ga	—	—				5902.871	0.3187	250.0
He				8.81×10^{-4}	2.56			
In	—	—				6141.774	0.3567	258.0
Ir	0.8435	1.6260	2.864					
K	0.054 24	0.497 67	6.369	0.114	4.285			
Kr				0.014	3.65			
Li				0.205	2.839			
Mo	0.7714	1.434	3.012	0.838	2.551			
N	10.56	2.557	1.097			5134.176	3.140	283.8
Na	0.063 34	0.589 93	5.336	0.1379	3.475			
Nb	0.9437	1.5501	3.079					
Ne				3.13×10^{-3}	2.74			
Ni	0.4279	1.3917	2.793	0.520	2.282			
O	5.12	2.68	1.208					
Pb	0.2455	1.2624	3.667	0.236	3.197			
Pd	0.4761	1.6189	2.89	0.427	2.52			
Pt	0.7102	1.6047	2.897	0.685	2.542			
Rb	0.046 44	0.429 81	7.207					
Rh	0.6674	1.5423	2.875					
Sr	0.1513	0.73776	4.988					
W	0.9710	1.385	3.053	1.068	2.562			
Xe				0.02	3.98			
AlN						698.647	0.3224	0.0
GaN						782.107	0.3166	0.0
InN						870.207	0.3263	0.0

i	c_i	d_i
	Moliere	
1	0.35	0.3
2	0.55	1.2
3	0.1	6.0
	ZBL	
1	0.028 17	0.201 62
2	0.280 22	0.402 90
3	0.509 86	0.942 29
4	0.181 75	3.199 80

3-body Potentiels but quasi pairwise screened Vashishta potential

$$\Phi = \phi_2 + \phi_3 = \sum_{i<j} U_{ij} + \sum_{i<j<k} W_{ijk} \,,$$

$$U_{ij} = \frac{H_{ij}}{r_{ij}^{\eta_{ij}}} + \frac{Z_i Z_j}{r_{ij}} e^{-r_{ij}/r_{1s}} - \frac{P_{ij}}{r_{ij}^4} e^{-r_{ij}/r_{4s}} \,,$$

$$H_{ij} = A_{ij}(\sigma_i + \sigma_j)^{\eta_{ij}} \,,$$

$$P_{ij} = \frac{1}{2}(\alpha_i Z_j^2 + \alpha_j Z_i^2) \,.$$

f radius is r_c.

$$W_{ijk} = B_{ijk} f(r_{ij}, r_{ik})(\cos\theta_{ijk} - \cos\bar{\theta}_{ijk})^2 \,,$$

$$f(r_{ij}, r_{ik}) = \exp\left(\frac{l}{r_{ij} - r_{c3}} + \frac{l}{r_{ik} - r_{c3}}\right) ; \quad r_{ij}, r_{ik} < r_{c3} \,,$$

$$\cos\theta_{ijk} = \frac{\mathbf{r}_{ik} \cdot \mathbf{r}_{ij}}{r_{ij} r_{ik}} ; \quad r_{ij}, r_{ik} < r_{c3} \,.$$

	A_{ij} (erg)	r_{1s} (Å)	r_{4s} (Å)	r_c (Å)	ℓ (Å)	r_{c3} (Å)
SiO_2	1.242×10^{-12}	4.43	2.5	5.5	1.0	2.6
Si_3N_4	2.00×10^{-12}	2.5	2.5	5.5	1.0	2.6
	σ_i (Å)	Z_i (e)	α_i (Å^3)			
Si	0.47	1.20	0.00			
O	1.20	−0.60	2.40			
Si	0.47	1.472	0.00			
N	1.30	−1.104	3.00			

	η_{ij}		B_{jik}(erg)	θ_{jik}(°)
Si–Si	11	Si–O–Si	3.20×10^{-11}	141.00
Si–O	9	O–Si–O	0.80×10^{-11}	109.47
O–O	7			
Si–Si	11	Si–N–Si	2.0×10^{-11}	120.00
Si–N	9	N–Si–N	1.0×10^{-11}	109.47
N–N	7			

P. Vashishta, & al, in Amorphous Insulators and Semiconductors, eds. M. F. Thorpe and M. I. Mithova, NATOASI Series 3, Vol. 23 (Kluwer, 1997), p. 151

N-body reactive potential
REBO family

$$V_{ij}(r_{ij}) = f_c\left(r_{ij}\right)\left\{V_R\left(r_{ij}\right) - b_{ij}\, V_A\left(r_{ij}\right)\right\}$$

$$V_A(r) = \frac{D_0}{S-1}\exp\left[-\beta\sqrt{2S}\,(r-R_0)\right],$$

$$V_R(r) = \frac{D_0 S}{S-1}\exp\left[-\beta\sqrt{\frac{2}{S}}\,(r-R_0)\right].$$

	Tersoff (Si)	Tersoff (C)	Brenner (C)	BN	NN	BB
D_0 (eV)	2.666	5.1644	6.325	6.36	9.91	3.08
R_0 (Å)	2.295	1.447	1.315	1.33	1.11	1.59
S	1.4316	1.5769	1.29	1.0769	1.0769	1.0769
β (Å^{-1})	1.4656	1.9640	1.5	2.043 057	1.927 871	1.524 4506
γ	1.1×10^{-6}	1.5724×10^{-7}	1.1304×10^{-2}	1.1134×10^{-5}	0.019 251	1.6×10^{-6}
n	0.787 34	0.727 51	1 ($1/2n = 0.804\,69$)	0.364 153 367	0.618 4432	3.992 9061
c	1.0039×10^5	3.8049×10^4	19	1092.9287	17.7959	0.526 29
d	16.217	4.384	2.5	12.38	5.9484	0.001 587
h	−0.598 25	−0.570 58	−1	0.5413	0	0.5
λ	0	0	0	1.9925	0	0
R (Å)	2.85	1.95	1.85	2.0	2.0	2.0
D (Å)	0.15	0.15	0.15	0.1	0.1	0.1

$$f_c(r) = \begin{cases} 1 & (r < R - D) \\ \frac{1}{2} - \frac{1}{2}\sin\left[\frac{\pi}{2}\frac{r-R}{D}\right] & R - D < r < R + D, \\ 0 & r \geqslant \end{cases}$$

$$b_{ij} = (1 + \gamma^n \chi_{ij}^n),$$

ou bien

$$f_c(r) = \frac{1}{1 + \exp[(r-R)/D]}.$$

$$\chi_{ij} = \sum_{k(\neq i,j)}^{N} f_c(r_{ik})\, g(\theta_{ijk}) \exp[\lambda^3 (r_{ij} - r_{ik})^3)],$$

$$g(\theta_{ijk}) = 1 + \frac{c^2}{d^2} - \frac{c^2}{d^2 + (h - \cos\theta_{ijk})^2}$$

Tight binding – 2nd moment approximation
(transition métals → catalysts)
True N-body potential : CPU time consuming

$$V_i = \sum_{i \neq j} A \exp\left[-p\left(\frac{r_{ij}}{r_0} - 1\right)\right] - \left\{\sum_{i \neq j} \xi^2 \exp\left[-2q\left(\frac{r_{ij}}{r_0} - 1\right)\right]\right\}^{1/2}$$

	Ni	Cu	Rh	Pd	Ag	Ir	Pt	Au	Al	Pb
A	0.0376	0.0855	0.0629	0.1746	0.1028	0.1156	0.2975	0.2061	0.1221	0.0980
ξ	1.070	1.224	1.660	1.718	1.178	2.289	2.695	1.790	1.316	0.914
p	16.999	10.08	18.45	10.867	10.928	16.980	10.612	10.229	8.612	9.576
q	1.189	2.56	1.867	3.742	3.139	2.961	4.004	4.036	2.516	3.648

Parametrized up to 5th neighbour

F. Cleri et V. Rosato, Phys. Rev B48 (1993) 22

Embedded Atom Method (EAM)

⇒ energy of a solid is a unique functional of the electron density.

⇒ uses the concept of electron (charge) density to describe metallic bonding:

⇒ each atom contributes through a spherical, exponentially-decaying field of electron charge, centered at its nucleus, to the overall charge density of the system.

⇒ Binding of atoms is modelled as embedding these atoms in this "pool" of charge, where the energy gained by embedding an atom at location r is some function of the local density.

⇒ The total energy thus writes:

$$E_{pot} = \sum_{i=1}^{N} E_i = \frac{1}{2}\sum_{i=1}^{N}\sum_{i,j,i\neq j}^{N}\phi_{ij}(r_{ij}) + \sum_{i=1}^{N} F_i(\rho_i) \qquad \rho = \sum_{j,j\neq 1}^{N} f_i(r_{ij})$$

With pairwise function:

$$\phi(r) = \frac{A\exp\left[-\alpha\left(\frac{r}{r_e}-1\right)\right]}{1+\left(\frac{r}{r_e}-\kappa\right)^{20}} - \frac{B\exp\left[-\beta\left(\frac{r}{r_e}-1\right)\right]}{1+\left(\frac{r}{r_e}-\lambda\right)^{20}} \qquad f(r) = \frac{f_e\exp\left[-\beta\left(\frac{r}{r_e}-1\right)\right]}{1+\left(\frac{r}{r_e}-\lambda\right)^{20}}$$

And the embedding function:

$$F(\rho)=\sum_{i=0}^{3}F_{ni}\left(\frac{\rho}{0.85\rho_e}-1\right)^i, \quad \rho<0.85\rho_e$$

$$F(\rho)=\sum_{i=0}^{3}F_{i}\left(\frac{\rho}{\rho_e}-1\right)^i, \quad 0.85\rho_e\le\rho<1.15\rho_e$$

$$F(\rho)=F_n\left[1-\eta\ln\left(\frac{\rho}{\rho_s}\right)\right]\left(\frac{\rho}{\rho_s}\right)^{\eta}, \quad \rho\ge1.15\rho_e$$

coupling rule

$$\phi^{ab}(r)=\frac{1}{2}\left[\frac{f^b(r)}{f^a(r)}\phi^{aa}(r)+\frac{f^a(r)}{f^b(r)}\phi^{bb}(r)\right]$$

reactive force field : ReaxFF
(based on distance angle relationship initially proposed by Tersoff/Brenner)

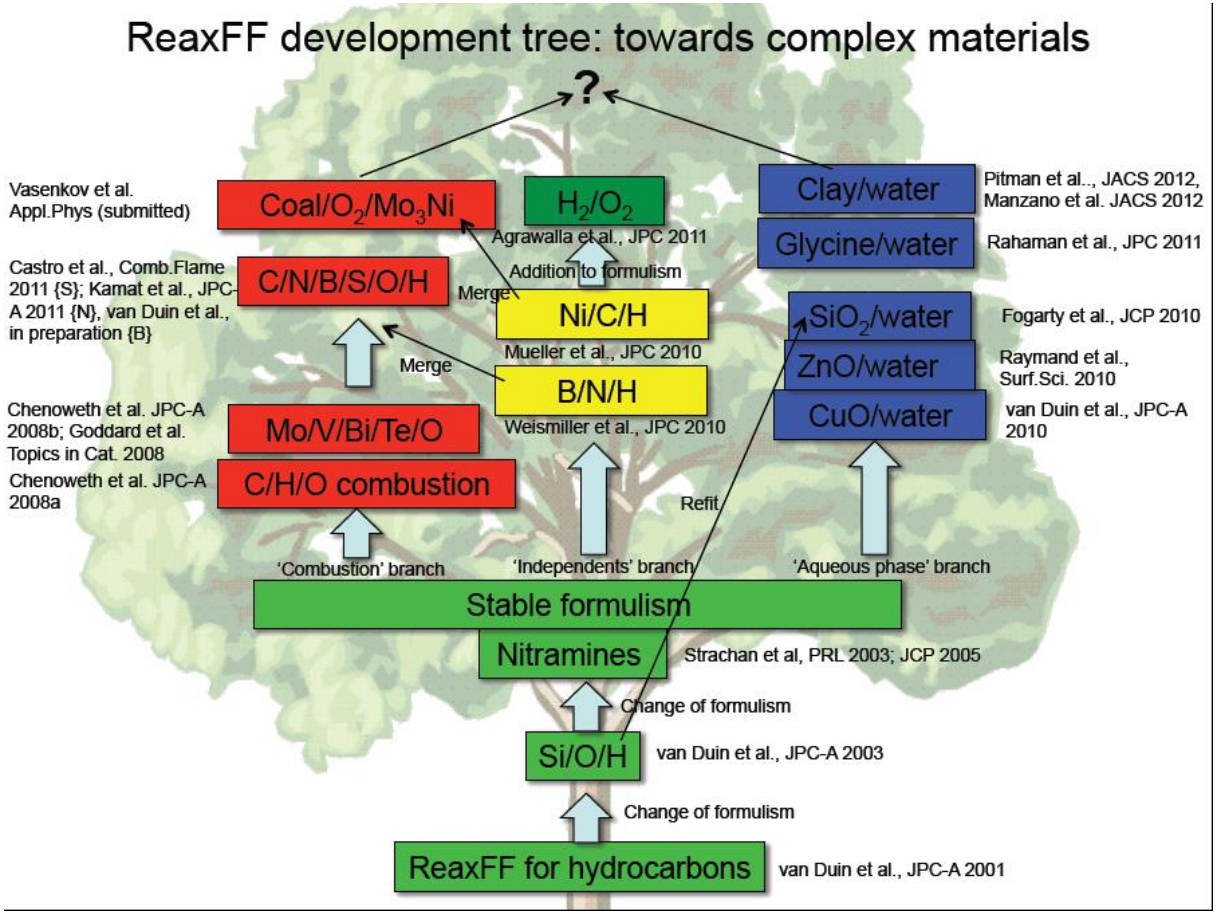

Charge Optimized Many Body (COMB) Potential :
adapted to reactive sputtering

Visual presentation of COMB potentials

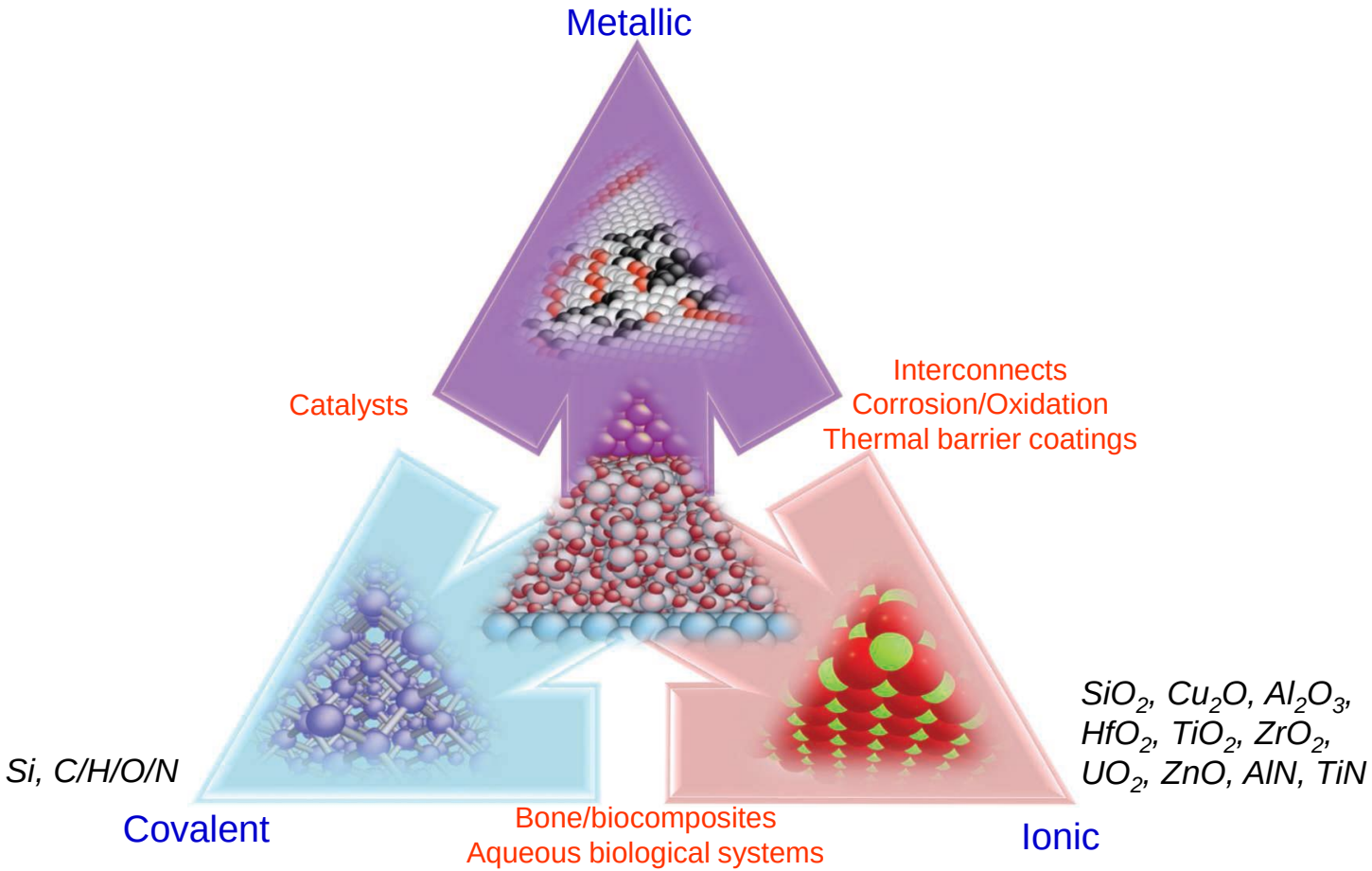

S. R. Phillpot, S. B. Sinnott, ***Science*** 325, 1634 (2009)

Functional form of COMB potential

- Functional form of COMB potential:
  - $$E_T = \sum_i \left[E_i^S(q_i) + \frac{1}{2}\sum_{j\neq i} V_{ij}\left(r_{ij}, q_i, q_j\right) + C(r_{ij}, q_i, q_j) \right]$$
  - Self energy: fit to atomic ionization energies and electron affinities

    $$E_i^S\left(q_i\right) = \chi_i q_i + (J_i + J_i^{field}) q_i^2 + K_i q_i^3 + L_i q_i^4$$
  - Interatomic potential: Charge dependent Tersoff + Coulomb

    $$V_{ij}(r_{ij}, q_i, q_j) = f_c(r_{ij}) \cdot A_{ij}(q_i, q_j) \cdot e^{-\lambda_{ij} \cdot r_{ij}} - f_c(r_{ij}) \cdot b_{ij} \cdot B_{ij}(q_i, q_j) \cdot e^{-\alpha_{ij} \cdot r_{ij}} + q_i \cdot J_{ij}(r_{ij}) \cdot q_j$$
  - Spherical charge distribution: 1*s*-type Slater orbital
    - $$J_{ij}(r_{ij}) = n_{ij} \int d^3 r_i \int d^3 r_j \; \rho_i(r_i, q_i) \rho_j(r_j, q_j) / r_{ij}$$
    - $$\rho_i(r_i, q_i) = q_i \frac{\xi_i^3}{\pi} \exp\left(-2\xi_i \left| r - r_i \right|\right)$$

[1] J. **Yu**, et. al., *Phys. Rev. B* 75 085311 (2007)
[2] T.-R. **Shan**, et al., Phys. Rev. B **81**, 125328 (2010)

Thermalisation model

As $\vec{F}.\vec{v} < 0$, or some relevant criterion, the velocity should be rescaled during some times $\Rightarrow$ thermostat

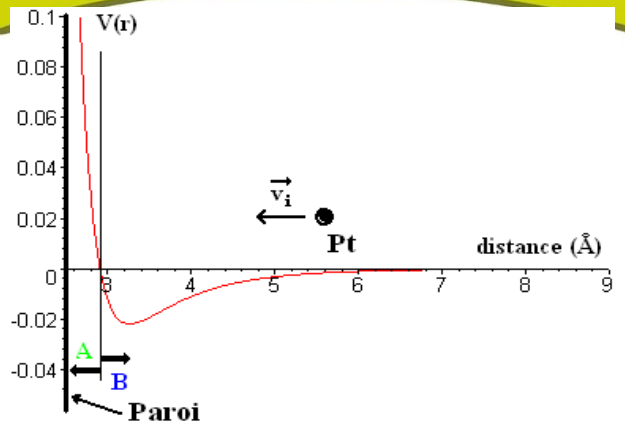

Collision is modelled by a coupling (electron-phonon, for metals) which introduces friction term in Newton equations of motion $\Rightarrow$ Langevin

$$\frac{\partial^2 \vec{r}_i(t)}{\partial t^2} = -\frac{1}{m_i}\frac{\partial}{\partial \vec{r}} V(\vec{r}_1(t), \vec{r}_2(t), \ldots, \vec{r}_N(t)) - \mu \vec{v}_i(t)$$

$$\mu = m_s \alpha \frac{T_i - T_e}{T_i} \quad et \quad \alpha = \frac{\Theta_D T_e L n e^2 k_B Z}{2 m_e \kappa \varepsilon_F}$$

α^{-1} is the thermalisation time

For example, Pt: α^{-1} = 1.17 ps
Au: α^{-1} = 20 ps

Q. Hou et al, Phys. Rev. B 62 (2000) 2825

other ways:

- velocity rescaling (Berendsen thermostat) :

v → χv with:

$$\chi = \left(1 + \frac{\mathrm{d}t}{\tau}\left(\frac{T_s}{T_k} - 1\right)\right)^{\frac{1}{2}}$$

τ is the thermal relaxation time.
T_s is the targeted temperature (surface),
T_k is the kinetic temperature: $E_k = kT_k \approx ½\ mv^2$

- Langevin thermostat :

$$m\ddot{\boldsymbol{r}}(t) = -m\Omega^2 \boldsymbol{r}(t) - \nabla_r W(\boldsymbol{r}, \boldsymbol{R}) - m\beta\dot{\boldsymbol{r}}(t) + \boldsymbol{f}(t),$$

$$M\ddot{\boldsymbol{R}}(t) = -\nabla_R W(\boldsymbol{r}, \boldsymbol{R}),$$

- Radial distribution function : Atom number between distances r and r+dr:

$$\int_0^\infty \rho g(r) 4\pi r^2 \, dr = N - 1 \approx N$$

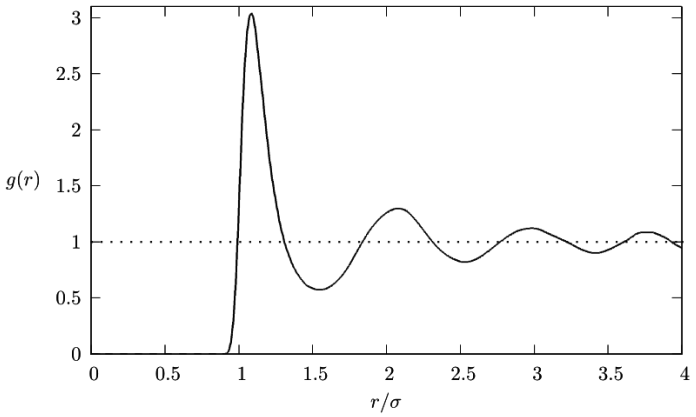

- Concentration profile of:
  - sputtering gas in the target, reactive species poisoning of the target
  - sputtered (reacted) materials on/in a substrate

- Size distribution (in flight or on a substrate)

- Diffusion coefficient : $D = \frac{1}{\delta} \lim_{t \to \infty} \frac{d\langle |r_i(t) - r_i(t_0)|^2 \rangle}{dt}$

- … many other things …

- Simulated X-ray patterns of:
  - (reactively) sputtered target
  - sputtered (reacted) film or clusters on/in a substrate

- Debye formula for calculating XRD patterns:

$$I_k(b) = \sum_n \sum_{n \neq m} f_n(b) f_m(b) \frac{sin(2\pi b r_{nm})}{2\pi b r_{nm}}$$

b=2sin(θ)/ λ and λ is the wavelength of the incident radiation, 2θ is the scattering angle, and r_{nm} is the distance between atoms n and m. The functions $f_n(b)$ and $f_m(b)$ are the scattering factors for atoms n and m, respectively

Pioneering work : H. M. Urbassek et al:

Molecular-dynamics simulation of sputtering

Herbert M. Urbassek

Fachbereich Physik, Universität Kaiserslautern, Erwin-Schrödinger-Straße, D-67663 Kaiserslautern, Germany

Nuclear Instruments and Methods in Physics Research B 122 (1997) 427–441

Boundary between low and high kinetic energy E_k = 100 eV ⇒ if > 100eV par repulsive potential (binary collision) as Molière, ZBL, Kr-C

Describe collision cascade E_k > 1 keV

Studies mostly concerned by Ion Beam Sputtering …

… a bit different than plasma sputtering

- lower energy range 10 to 500 eV
- buffer gas ⇒ collisions :
  - Energy distribution function is modified
  - molecules, clusters formation

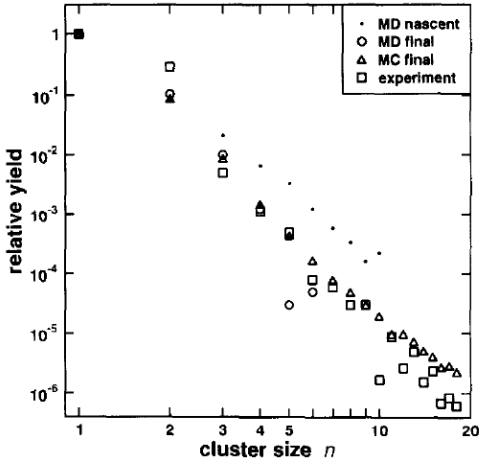

Fig. 5. Relative abundance distribution $Y(n)$ of Ag_n clusters sputtered from a Ag (111) surface due to 5 keV Ar bombardment. Nascent and final distributions calculated by molecular dynamics immediately after, and 500 ps after ion emission. Monte Carlo results, extrapolated from molecular-dynamics data as described in the text. Experimental data from Ref. [157]. Plotted after Ref. [59] with permission of the author.

Available computer codes

Table 1.1. Computer codes used in the fields of ion-implantation and ion-surface interactions

Slowing Down Process						Thermal Process
Binary Collision Approximation				Molecular Dynamics		Local Mixing
Simple MC		Dynamical MC				
ACAT[1]	ACOCT[5]	TRIDYN[10]	EVOLVE[12]	MDACOCT[24]	MD-TOPS[26]	Model
TRIM[2]	MARLOWE[6]	T-DYN[11]	dynamic-SASAMAL[13]	PARASOL[25]	SPUT2SI[29]	DIFFUSE[16]
TRIM.SP[3]	Crystal-TRIM[7]			MODYSEM[27]	SPUT3[28]	PIDAT[17]
SASAMAL[4]	COSIPO[8]	DynamO : http://dynamomd.org/		MOLDYCASK[30]	QDYN[32]	
	IMSIL[9]			MOLDY[31]	REED[33]	
		DYACAT[14]	DYACOCT[15]			
		ACAT-DIFFUSE[19] ACAT-DIFFUSE-GAS[20] EDDY[23] TMAP4[18] TRIDYN+PIDAT[21] TRIDYN+DIFFUSEDC+YCEHM[22]				

(1) Y. Yamamura and Y. Mizuno, Research report of Institute of Plasma Physics, Nagoya University IPPJ-AM-40 (1985).
(2) J.P. Biersack and L.G. Haggmark, Nucl. Instr. Meth. 174 (1980) 257.
(3) J.P. Biersack and W. Eckstein, Appl. Phy. A34 (1984) 73.
(4) Y. Miyagawa and S. Miyagawa, J. Appl. Phys. 54 (1983) 7124.
(5) Y. Yamamura and W. Takeuchi, Nucl. Instrum. Methods B29 (1987) 461.
(6) M.T. Robinson and I.M. Torrens, Phys. Rev. B9 (1974) 5008.
(7) M. Posselt, Radiat. Eff. Def. Solid. 130/131 (1994) 87.
(8) M. Hautala, Phys. Rev. B30 (1984) 5010.
(9) G. Hobler, H. Potzl, L. Gong and H. Ryssel, in: Simulation of Semicondoctor Devices and Process, eds. W. Fichtner and D. Aemmer, Vol. 4 (Hartung-Gorre, Konstanz, 1991) p.389.
(10) W. Möller and W. Eckstein, Nucl. Instr. Meth. B 2 (1984) 814.
(11) J.P. Biersack, S. Berg and C. Nender, Nucl. Instr. Meth. B59–60 (1991) 21.
(12) M.L. Roush, T.S. Andreadis and O.F. Goktepe, Radiat. Eff. 55 (1981) 119.
(13) Y. Miyagawa, M. Ikeyama, K. Saitoh, G. Massouras, S. Miyagawa, J. Appl. Phys. 70 (1991) 7289.
(14) Y. Yamamura, Nucl. Instrum. Methods B33 (1988) 493.
(15) Y. Yamamura, I. Yamada and T. Takagi, Nucl. Instr. Meth. B37–38 (1989) 902.
(16) K.L. Wilson and M.I. Baskes, J. Nucl. Mater. 76/77 (1978) 291.
(17) W. Möller, Max-Plank-Institute für Plasmaphysik, Report IPP 9/44 (1983).
(18) G.R. Longhurst, D.F. Holland, J.L. Jones, B.J. Merrill, TMAP4 User's Manual, EGG-FS-10315, Idaho National Engineering and Environmental Laboratory, 1992.
(19) Y. Yamamura, Nucl. Instr. Meth. B 28 (1987) 17.
(20) M. Ishida, Y. Yamaguchi and Y. Yamamura, Thin Solid Films 334 (1998) 225.
(21) W. Eckstein, V.I. Shulga, J. Roth, Nucl. Instr. Meth. B 153 (1999) 415.
(22) K. Schmid and J. Roth, J. Nucl. Mater. 313–316 (2003) 302.
(23) K. Ohya and R. Kawakami, Jpn. J. Appl. Phys. 40 (2001) 5424.
(24) K. Yorizane, T. Muramoto and Y. Yamamura, Nucl. Instr. Meth. B153 (1999) 292.
(25) G. Betz, R. Kirchner, W. Husinsky, F. Rudenauer and H.M. Urbassek, Radiation Effects and Defects in Solids 130/131 (1994) 251.
(26) Javier Domínguez-Vázquez, E. Pablo Andribet, A. Mari Carmen Pérez-Martín, José J. Jiménez-Rodríguez, Radiation Effects and Defects in Solids 142 (1997) 115.
(27) V. Konoplev and A. Gras-marti, Philosophical magazine A71 (1995) 1265.
(28) M.H. Shapiro and T.A. Tombrello, Nucl. Instr. Meth. B84 (1994) 453.
(29) M.H. Shapiro, T.A. Tombrello and D.E. Harrison, Jr., Nucl. Instr. Meth. B30 (1988) 152.
(30) T. Diaz de la Rubia and M.W. Guinan, J. Nucl. Mater. 174 (1990) 151.
(31) B.L. Holian, The MOLDY program is filed in mass storage at the Los Alamos National Laboratory (1975).
(32) D.E. Harrison, Jr. and M.M. Jakas, Radiat. Eff. 99 (1986) 153.
(33) Jeong-Won Kang, E.S. Kang, M.S. Son, and H.J. Hwang, Journal of Vacuum Science & Technology B18 (2000) 458–461.

reprinted from: T. Ono et al, in Reactive Sputter Deposition SSMS 109, D. Depla & S. Mahieu Ed., Berlin, 2008, pp. 1-42

To what we have to pay special care in addition to the interaction potentials

Ion flux :

Exp. 1 10^{17}cm^{-2} s^{-1} (*)= 10 ions / 10x10 nm^2 / s (*) 1A on 4'' target

MD 1 ions/10x10 nm^2/2 ps

Integration timestep dt

Evolves as $dt = \frac{C}{\sqrt{\max_{1 \le i \le N}\left(\frac{2[E_{kin} + \max(0, V_i)]}{m_i}\right)}}$ (E < 1eV : dt ≈ 1 fs, except quick motion bound H 0.1 fs)

Thermal relaxation

- Choose a relevant ion realease time: i.e. greater than thermalisation time
- Choose a relevant thermostat (region i.e. what should thermostated) with this relevant time
- For sputtering one can guess that only the substrate should be thermostated

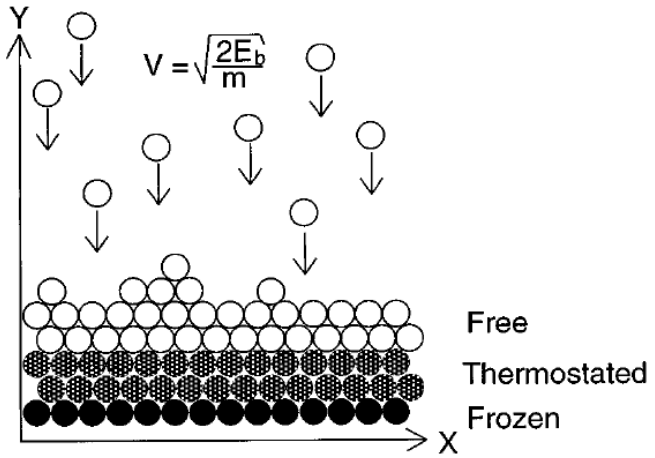

NB a neutral-atom potential is appropriate because the incident ion is neutralized well before impact by a fast Auger process or resonant charge transfer

Molecular Dynamics Simulations
Sputtering: effect of the potential

B.J. Thijsse et al. / Applied Surface Science 231–232 (2004) 29–38

Molecular dynamics simulation of silicon sputtering: sensitivity to the choice of potential

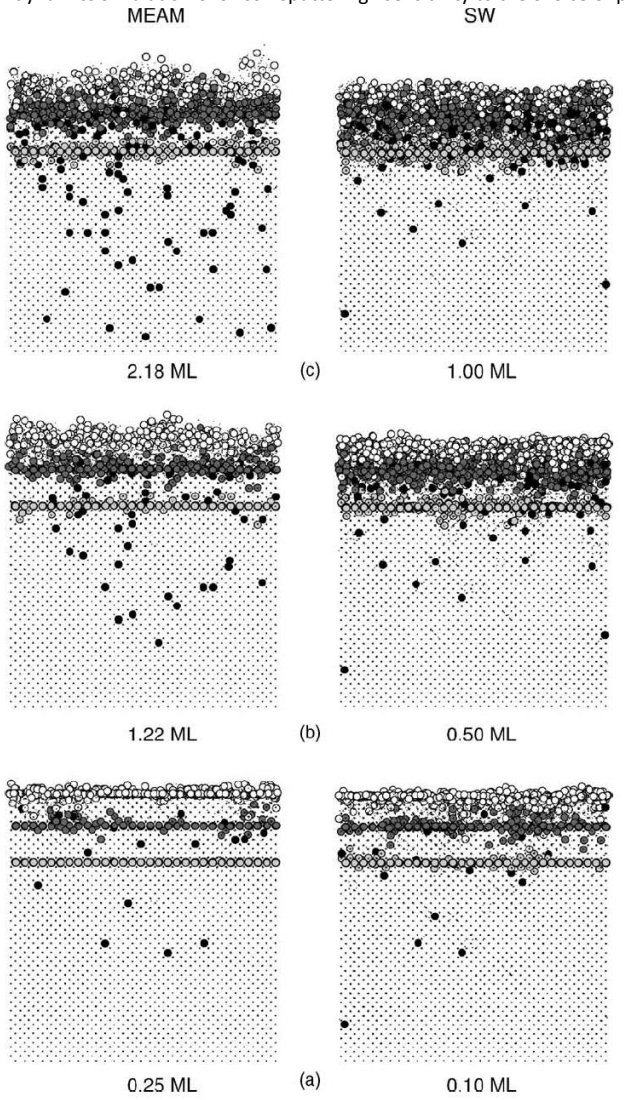

Side-view snapshots of Si(001) targets irradiated by 500 eVAr atoms at 45° incidence, with doses (bottom to top): (a) 0.48 10^{14} Ar/cm^2, (b) 2:14 10^{14} Ar/cm^2, and (c) 4:26 10^{14} Ar/cm^2.

The white, dark gray, and light gray circles represent the atoms initially in planes 1, 8, and 17, respectively (counted from the top),

and the black circles are implanted Ar atoms.

All other atoms are represented by small dots.
The left column shows the MEAM simulation results, the right column the SW results. Under each snapshot the number of sputtered monolayers is indicated.

SW Stillinger-Weber : Tersoff-like potential
MEAM Modified EAM for including bond angles

Molecular Dynamics Simulations
Sputtering: effect of the potential

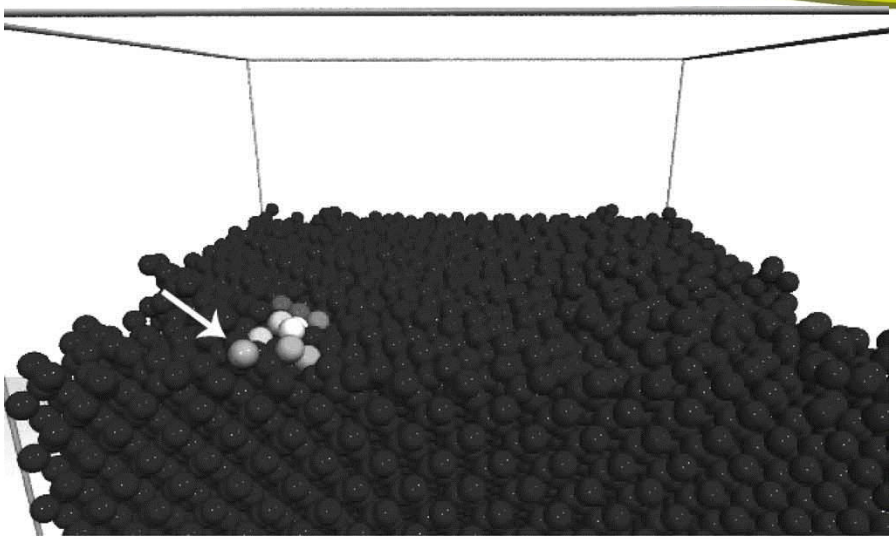
(a)

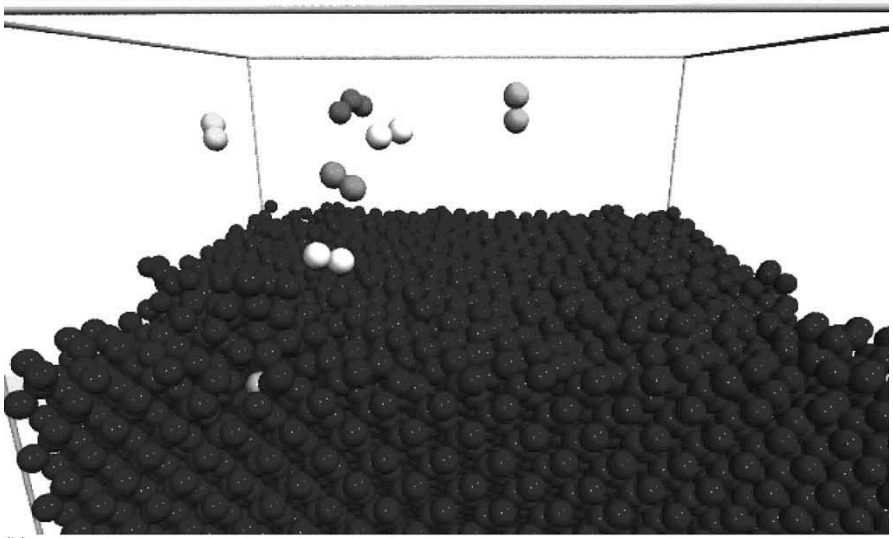
(b)

Sputter burst event occurring in the MEAM simulation:
(a) situation just before Ar impact (arrow), highlighting the 13 Si atoms that will eventually be sputtered;

(b) five Si dimers and one Si trimer ejected from the surface. The Ar atom is still visible in the surface region.

MEAM fitted to DFT results, but spurious thermal effects are occuring.
Lesson : even when using potentials that are well fitted to first-principles data, one should be extremely cautious and never stop validating (experimentally) results.

Molecular Dynamics Simulations
Sputtering: sputtered atom data

Molecular dynamics simulation of Cu and Ar ion sputtering of Cu (111) surfaces
J. D. Kress, D. E. Hanson, A. F. Voter, C. L. Liu, X.-Y. Liu, and D. G. Coronell, JVST A 17, 2819 (1999)

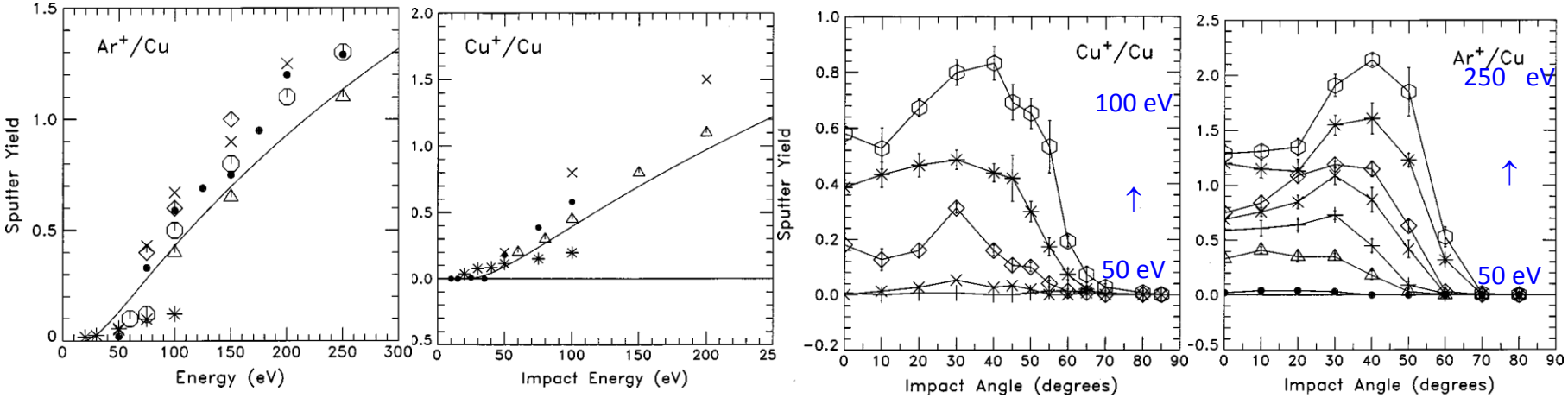

Experiments (o, Δ, ◊), empirical formula (–), binary collision (*) previous MD simulation (x); present MD (•)

Comparison with experiment (Δ), the formula of Yamamura *et al.* (–), the present MD simulation (•), the MD simulation of Shapiro and Tombrello (x), and binary collision simulation (*)

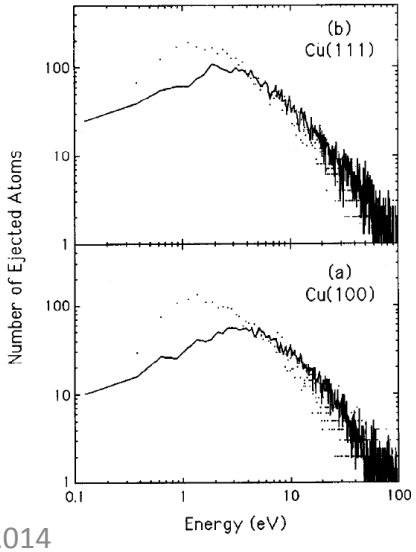

Energy distributions
… pair potential
– EAM potential

Potentials
Cu – Cu : EAM
Ar – Cu : ZBL
Ar – Ar : Molière.

Molecular Dynamics Simulations beyond magnetron sputtering (I)

Helium interaction with tungsten

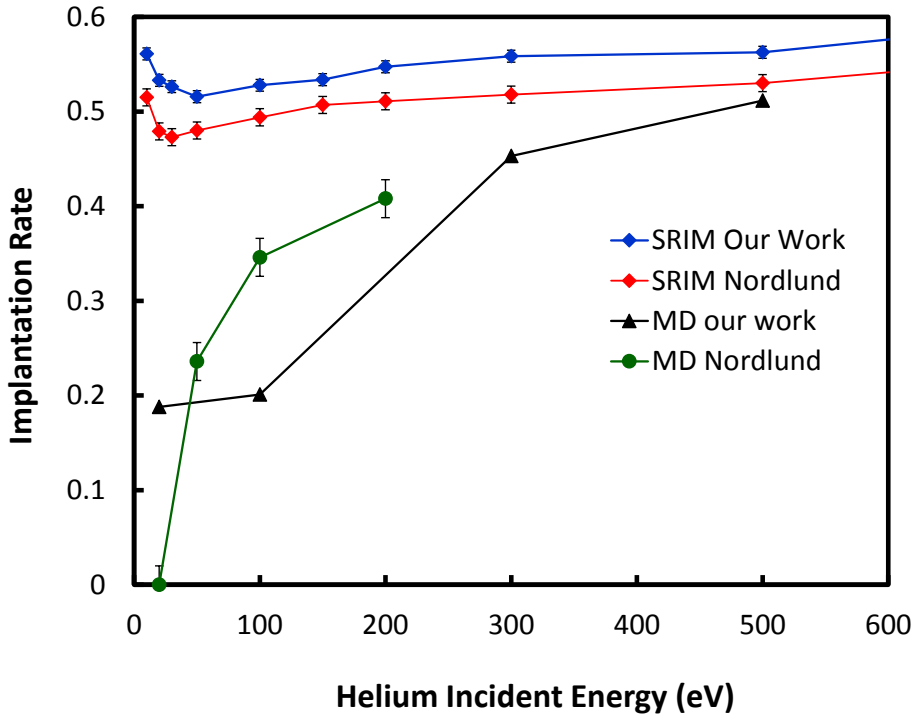

Discrepancy between Md and SRIM at low enrgies.
Discrepancy between MDs : HeW potentials

Our Work: Ph D thesis work of L. Pentecoste at GREMI

Nordlund: K.O.E. Henriksson, K. Nordlund, J. Keinonen , Molecular dynamics simulations of helium cluster formation in tungsten, Nuclear Instruments and Methods in Physics Research B 244 (2006) 377–391

He bubble formation and W flaking off

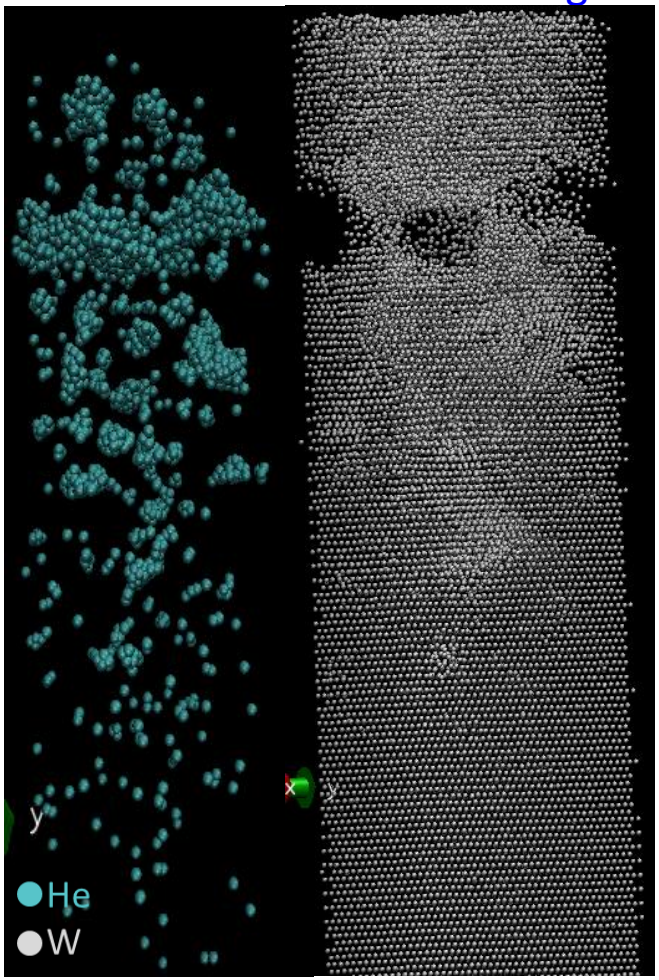

Molecular Dynamics Simulations beyond magnetron sputtering (II)

Sputter etch: compound sputtering → Ar^+ on GaAs

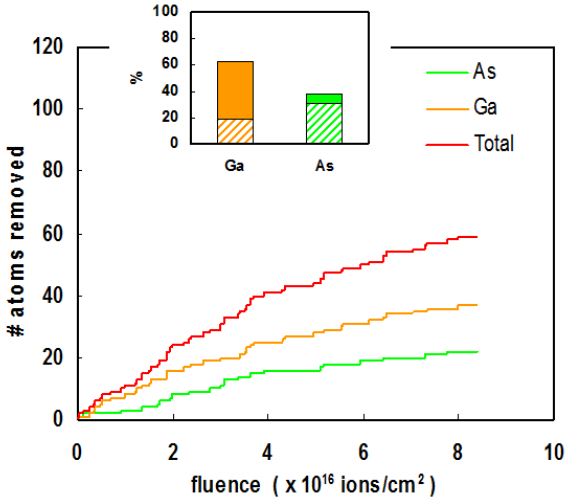

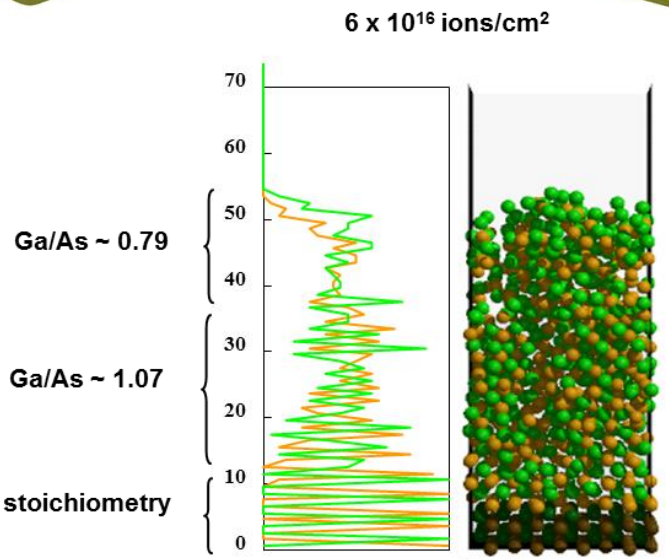

- Ga preferential sputtering and As cross-linking initially occur on top surface
- More than 97% of sputtered species are single atoms, in good agreement with experimental mass spectrometry studies*
- Thermal desorption is necessary to get steady state

- Concentration profiles show a top surface enrichment of As, a subsurface depletion of As, then a return to stoichiometry deeper in the solid
- Good agreement with ARXPS and AES analyses* of GaAs surfaces exposed to higher bombardment energies [0.5;5keV] but with Ga/As ratios closer to unity

Emilie Despiau-Pujo, Pascal Chabert, and David B. Graves, Molecular dynamics simulations of GaAs sputtering under low-energy argon ion bombardment, JVST A 26, 274 (2008)

Molecular Dynamics Simulations reactive magnetron sputtering

None about this topics except reactive ion etching !!

Why ?

1/ complicated :

reactive species: neutral, radical, dissociation, ionisation

Target poisoning

molecule formation with sputtered materials

2/ problem with time and length scales

especially for reactivity during transport to substrate

-

3/ Availability of metal-oxide, nitride, carbide potentials

COMB (TiO, N_x, SiO_x, AlO_x, HfO_x, ZnO, …)

and REBO (B, C, H, N, Si, O)

and ReaxFF (C, H, N, Si, O)

4/ how to ?

Ion flux: 1. $10^{17}cm^{-2}s^{-1}$ $\Rightarrow \frac{n_n}{n_i}$ above the surface ≈ 1 to 100

reactive neutral flux: few $10^{17}cm^{-2}s^{-1}$

Problem : how to describe molecule formation ?

Trick: use P.d of the experiment and increase P and decrease d accordingly

collison number being $\propto$ P.d

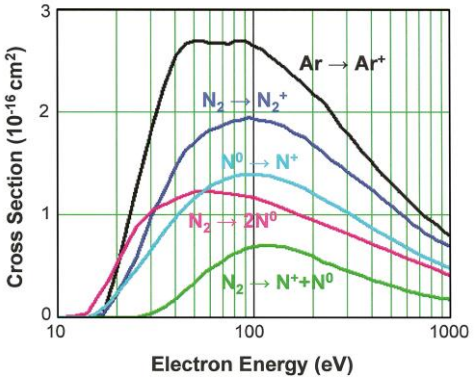

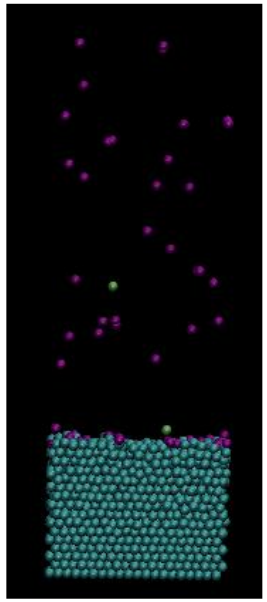

Molecular Dynamics Simulations
Condensation during the flight

If gas pressure large enough (as for gas condensation) clustering of sputtered atoms occurs during the flight to the surface

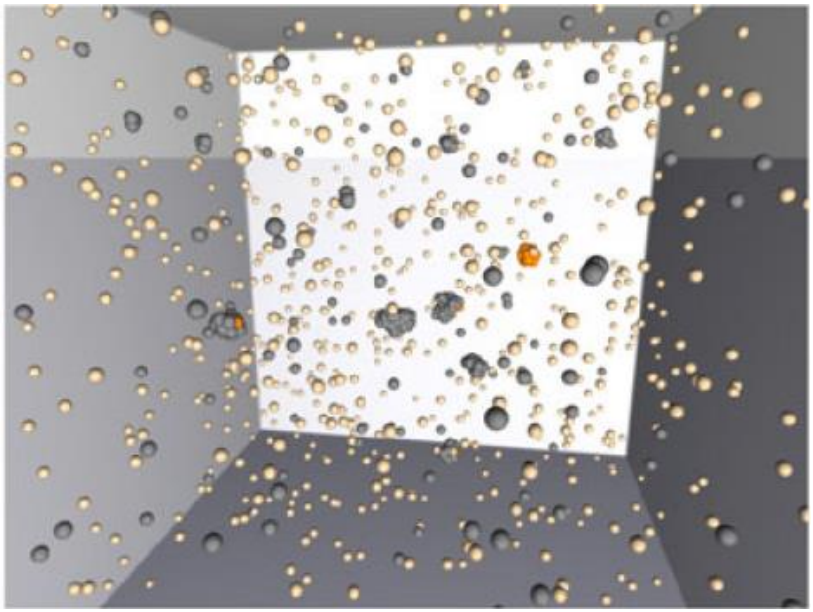

Snapshots of a simulation (800 K inert gas temperature, Ar:Fe 2:1, ρ(Fe) = 0.07 mol dm^{-3}) after 2.3 ns simulation time. Beige: argon; grey: iron in unordered structures, orange: iron in an icosahedral environment.

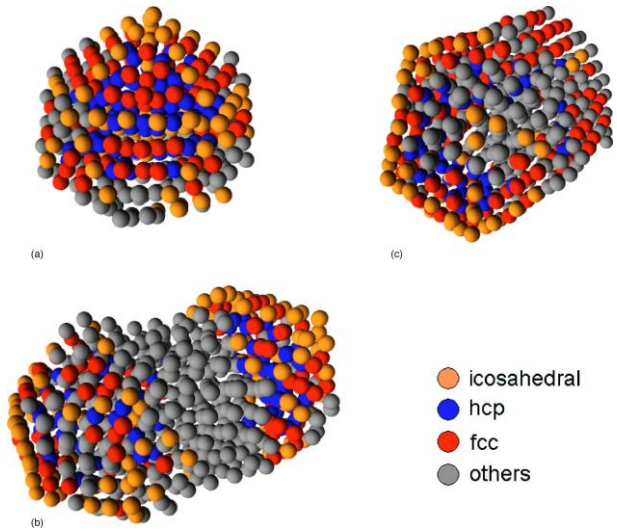

(a) The biggest cluster before the collision. (b) The new cluster 0.165 ns after the collision or at 16.4 ns of the overall simulation time. (c) The cluster at 11.3 ns after the collision or 27.5 ns of the overall simulation time.

N Lümmen, T Kraska, Investigation of the formation of iron nanoparticles from the gas phase by molecular dynamics simulation, Nanotechnology 15 (2004) 525–533; Molecular dynamics investigations of the coalescence of iron clusters embedded in an inert-gas heat bath, Phys. Rev B 71 (2005) 205403

Focus on complex materials: metallic glass , high entropy alloys and metal oxides

recall: Energy distribution of incoming species at the substrate position .

$$f(E) \propto \frac{1-\left(\frac{E_{coh}+E}{\Lambda E_{Ar^+}}\right)^{\frac{1}{2}}}{E^2\left(1+\frac{E_{coh}}{E}\right)^3}$$

$$E_F = \left(E - k_B T_g\right)\exp\left[n\ln\left(E_f / E_i\right)\right] + k_B T_g$$

$$n = \frac{d_{T-S} P \sigma}{k_B T_g}$$

MD flux: 1 at/100nm^2/2ps i.e. 0.5 at nm^{-2} ps^{-1}
Exp flux: 10^{15}at cm^{-2}s^{-1} i.e. 10 at nm^{-2}s^{-1} !

So time between releasing each depositing atoms should be greater than thermalisation time : a few ps

Released total number: 10000 at.

Metallic Glass Zr_xCu_{100-x} deposition

Experiment	Zr (eV)	Cu (eV)	Experiment Conditions
1	7.65	6.67	d_{T-S}= 9 cm, P = 0. 25 Pa, Target bias = 300 V
2	12.6	9.61	d_{T-S} = 7 cm, P = 0.03 Pa, Target bias (Zr) = 460 V, Target bias (Cu) = 490 V
3	0.13	0.34	d_{T-S} = 7 cm, P = 3 Pa, Target bias (Zr) = 460 V, Target bias (Cu) = 490 V

Composition

A « vapor » is created with the appropriate composition, in which an atom can be selected with random position and velocity selected in the relevant distribution.

Differences between vapor and targeted composition inform about differential sticking

→ 10000 released atoms, around 7000-9000 stick with the targeted composition.

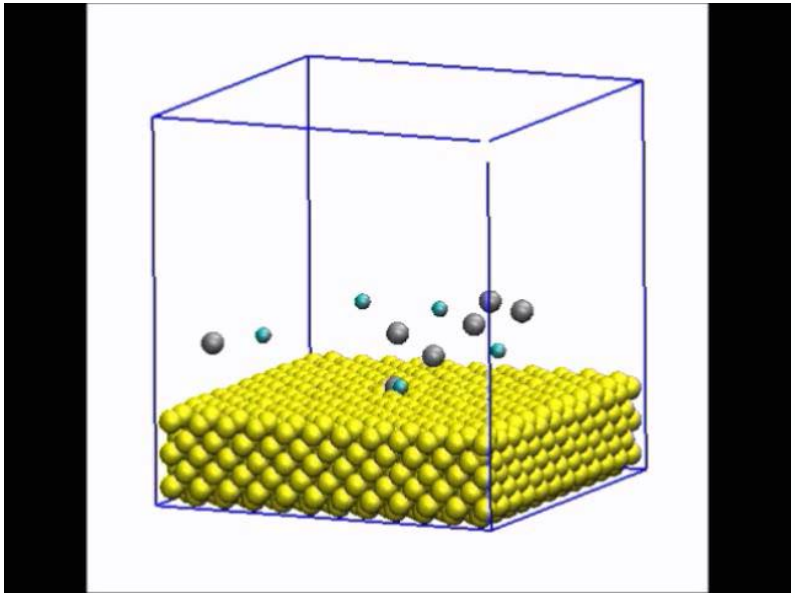

$Zr_{46}Cu_{54}$ (3265/3765)

Zr_xCu_{100-x} Snapshots

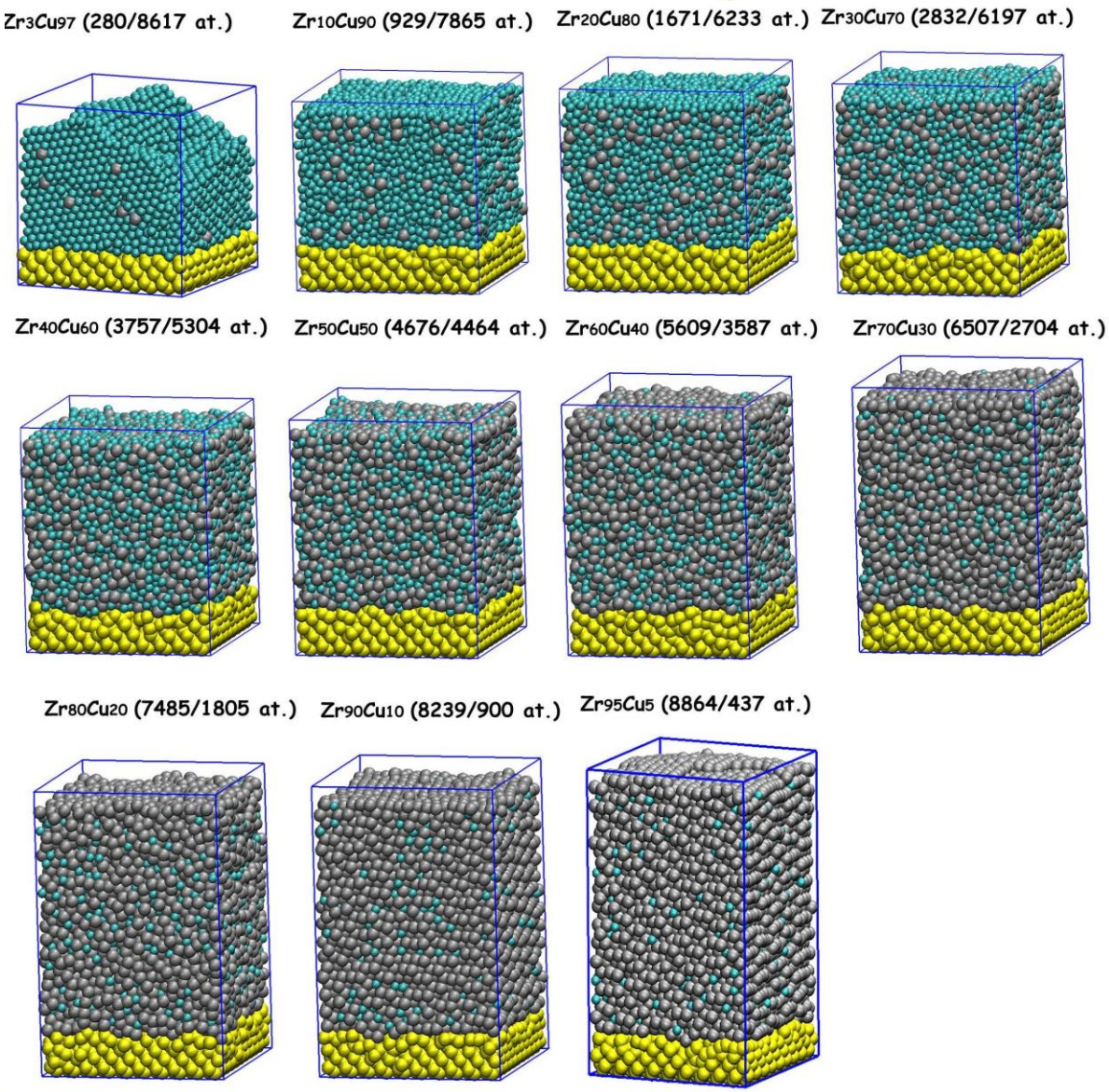

Zr_xCu_{100-x} Radial Distribution Functions

Crystal name	Structure	First neighbor (Å)	Second neighbor (Å)	Third neighbor (Å)	Fourth neighbor (Å)
Zr	HCP	3.20	4.53	5.15	5.57
Cu	FCC	2.55	3.61	4.43	5.11

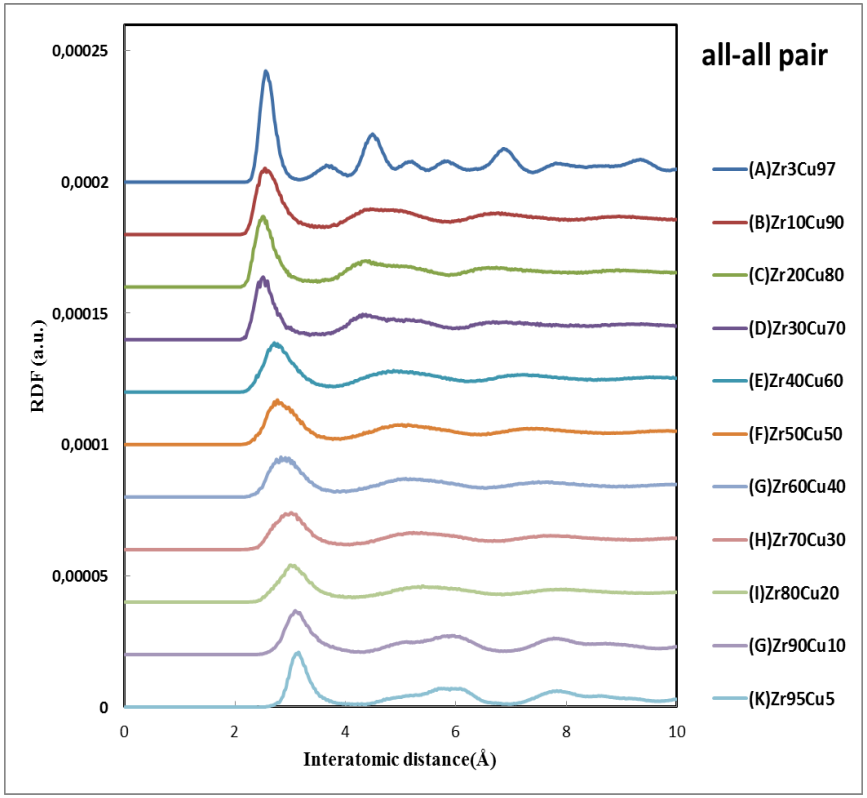

Amorphous structure on a wide range as observed in the experiments

Zr_xCu_{100-x} X-Ray diffraction

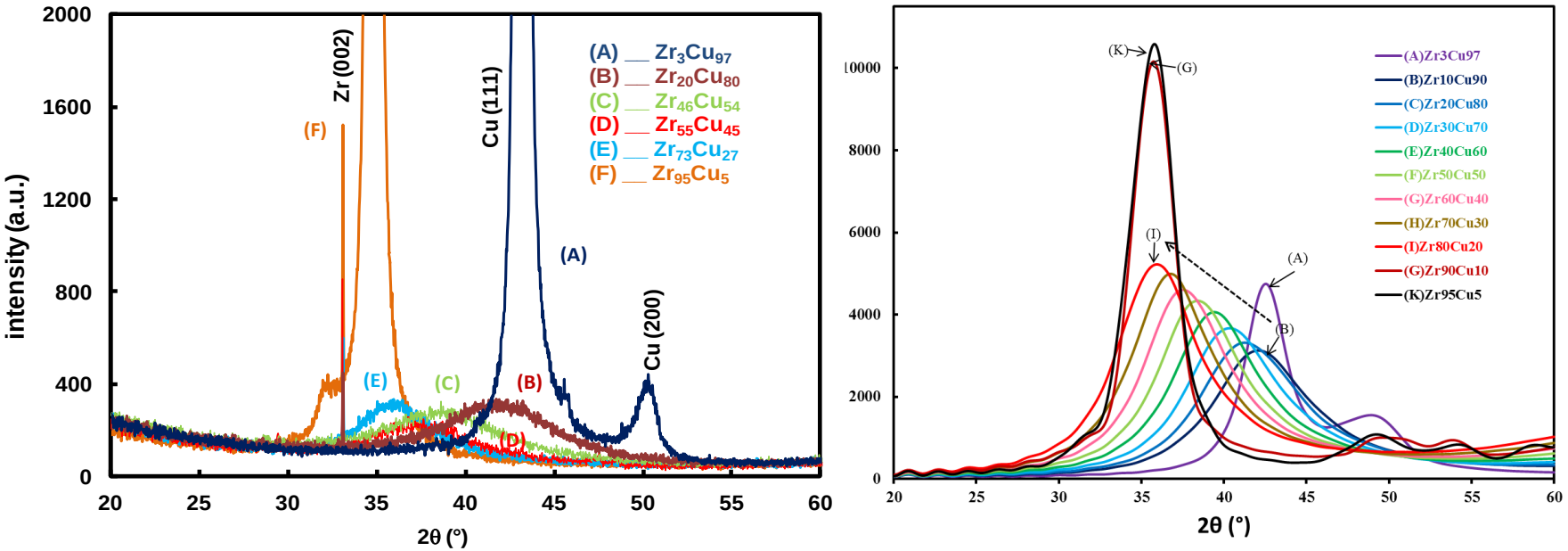

Experimental and simulated X-Ray diffraction patterns. MD correctly reproduces the transition from Zr to Cu rich experimental XRD pattern evolution.

Lu Xie, Pascal Brault, Anne-Lise Thomann, Larbi Bedra , Molecular dynamic simulation of binary Zr_xCu_{100-x} metallic glass thin film growth, Appl. Surf. Sci. **274** (2013) 164–170

L. Xie, P. Brault, J.-M. Bauchire, A.-L. Thomann, L. Bedra , Molecular Dynamics simulations of clusters and thin film growth in the context of plasma sputtering deposition, J. Phys D 47 (2014) 224004 (invited article)

Experiment	Zr (eV)	Cu (eV)
1	7.65	6.67
2	12.6	9.61

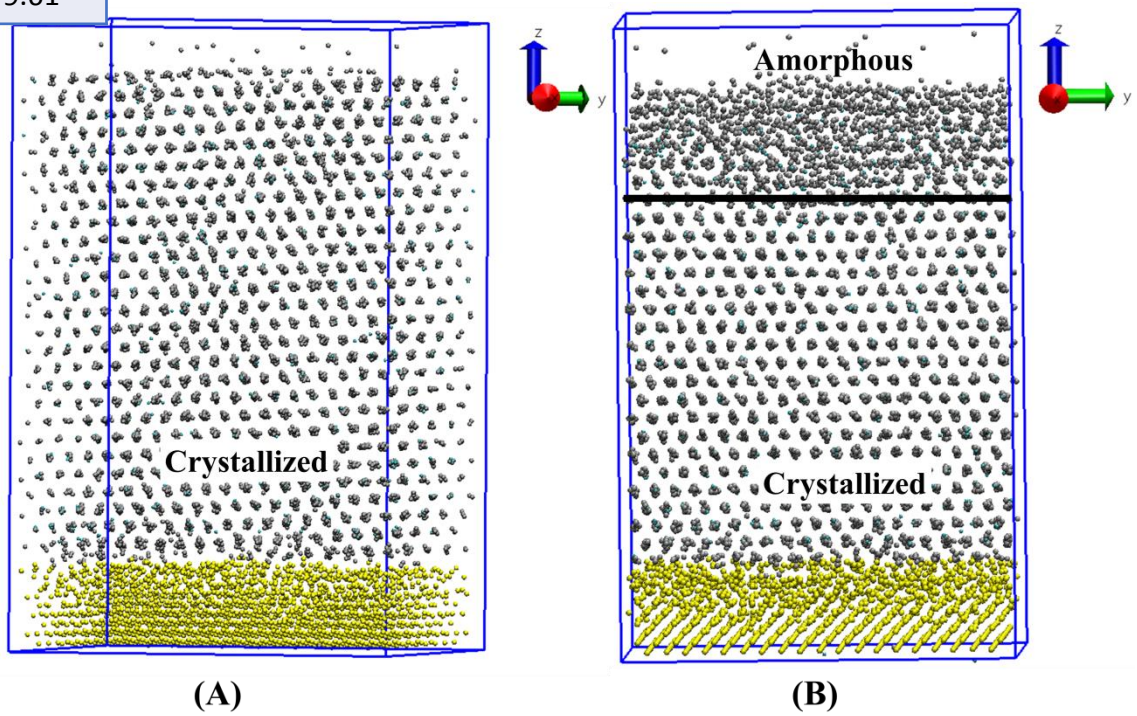

Snapshots of $Zr_{90}Cu_{10}$ in experiment 1 (A) and experiment 2 (B) deposited on Si(100) substrate with their specific orientation showing the crystal structure. Solid line in B is used to separate the amorphous and crystalline structures. Excess Energy serves as amorphization of the film top

Zr_xCu_{100-x} Low energies : condition 3

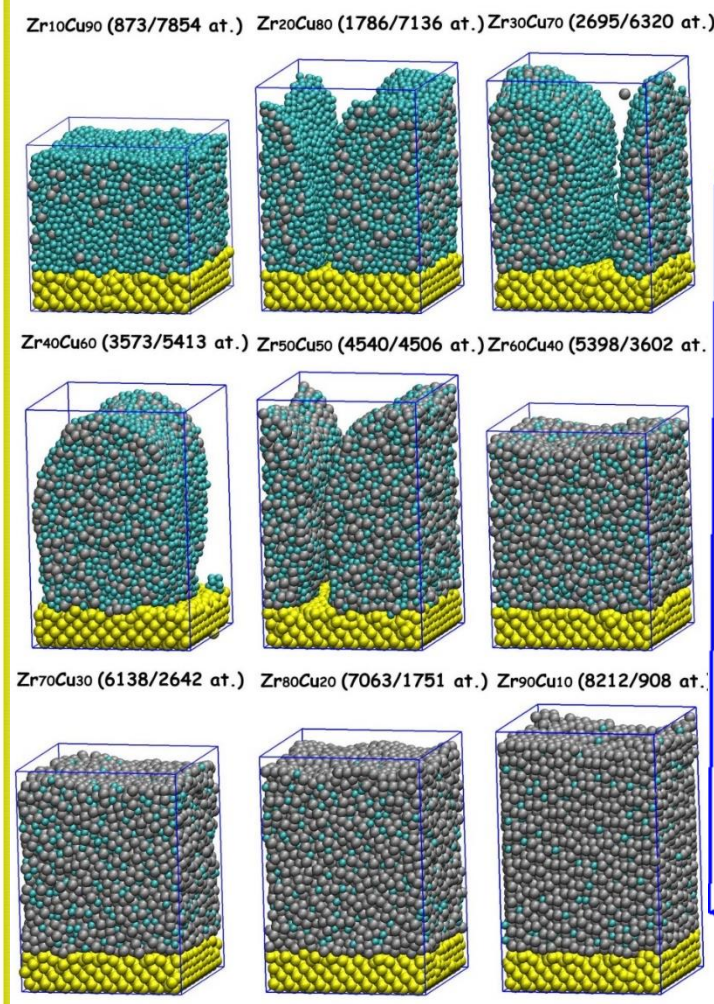

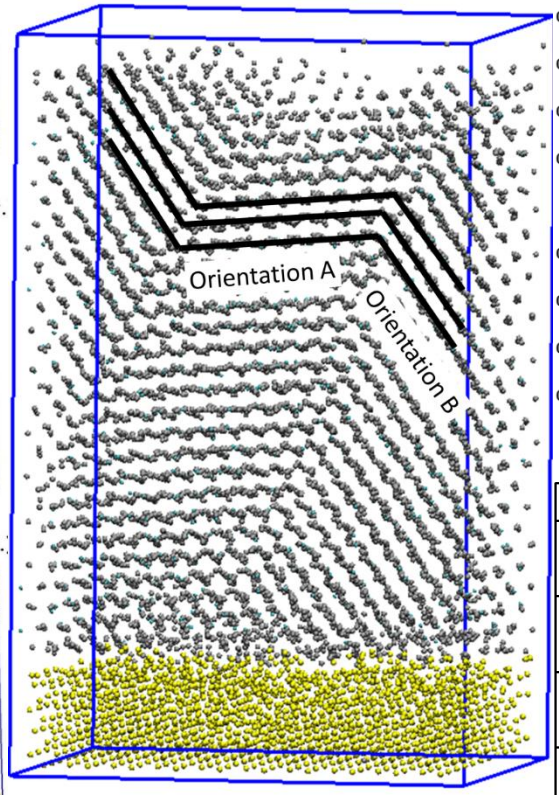

$Zr_{90}Cu_{10}$

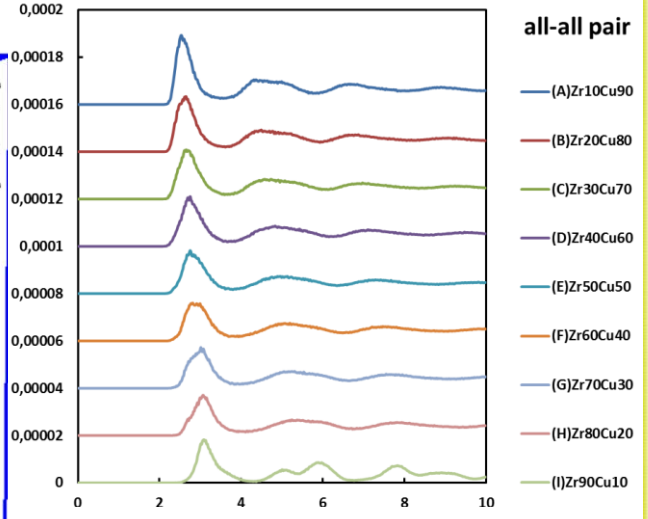

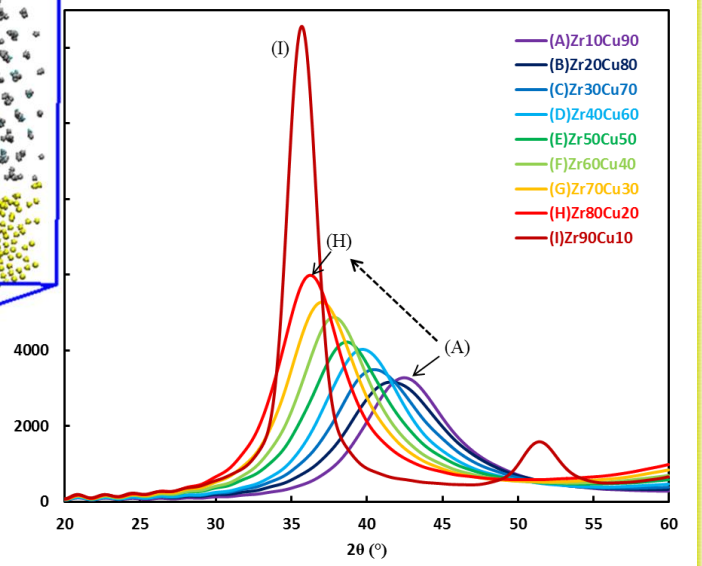

Experiment	Zr (eV)	Cu (eV)
3	0.13	0.34

Low energy: polycrystalline

HEA : AlCoCrCuFeNi
Thin film growth

Al, Co, Cr, Cu, Fe, Ni, Si

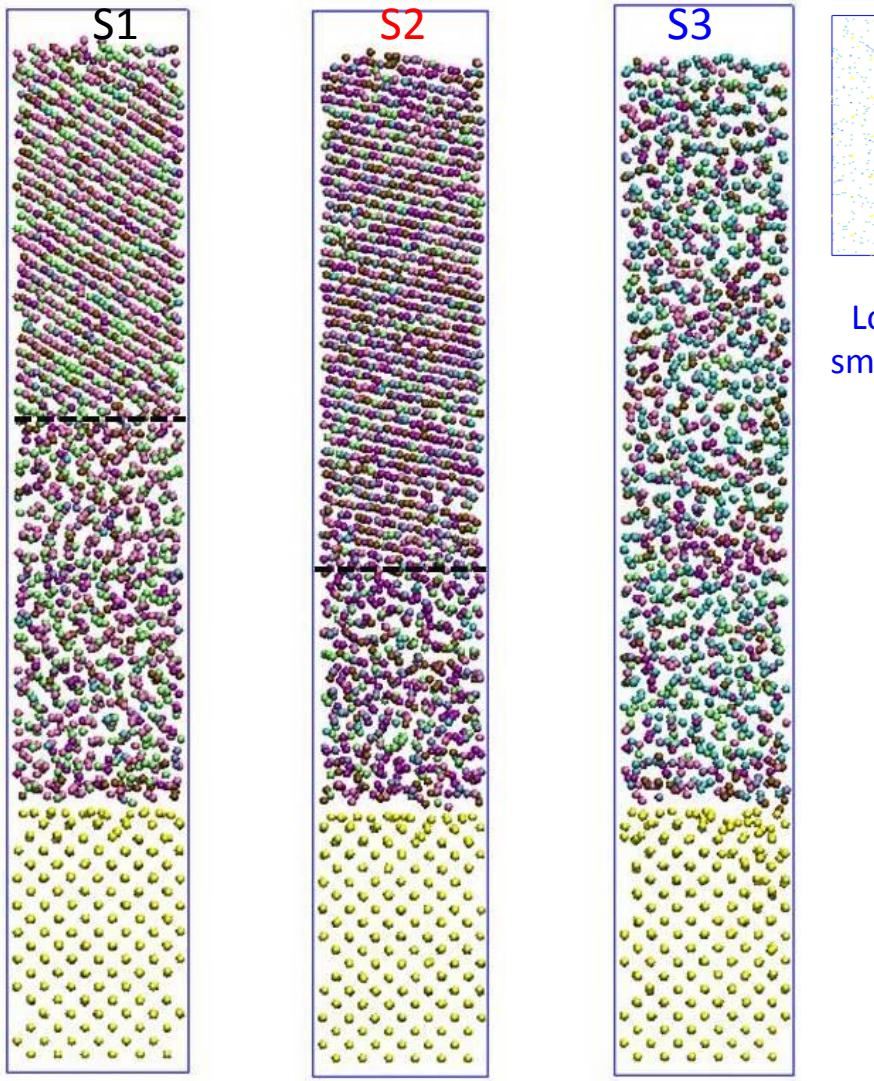

$Al_2Co_9Cr_{32}Cu_{39}Fe_{12}Ni_6$ $Al_3Co_{26}Cr_{15}Cu_{18}Fe_{20}Ni_{18}$ $Al_{39}Co_{10}Cr_{14}Cu_{18}Fe_{13}Ni_6$

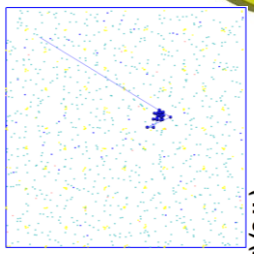

Low diffusion
small substrates
⇓
thin film

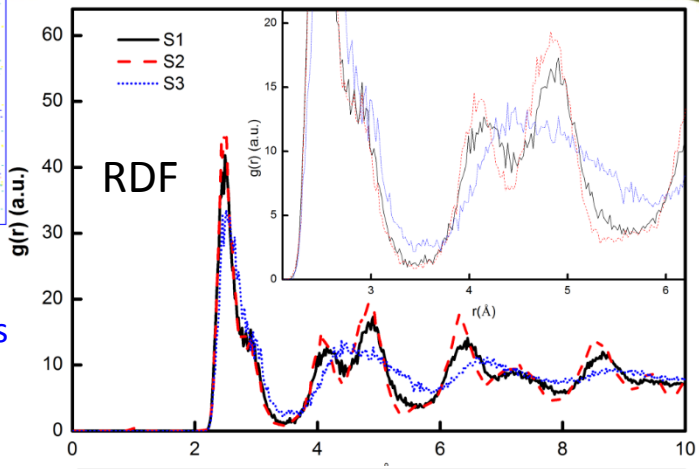

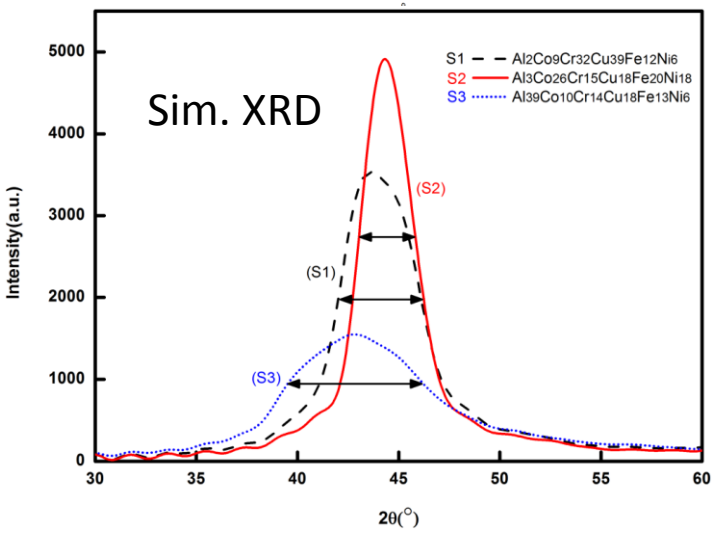

Composition => Important effect on the structure

L. Xie, P. Brault, J.-M. Bauchire, A.-L. Thomann, L. Bedra , Molecular Dynamics simulations of clusters and thin film growth in the context of plasma sputtering deposition, J. Phys D 47 (2014) 224004

HEA: AlCoCrCuFeNi
Deposition and Annealing from 25 to 1200°C

quasi equimolar AlCoCrCuFeNi deposition:

1309/1205/1293/1357/1348/1354 atoms → $Al_{17}Co_{15}Cr_{17}Cu_{17}Fe_{17}Ni_{17}$

<E> = 1 eV for each element

Sticking = 0.80 env.

Substrate Si(100) ≈100x100 $Å^2$

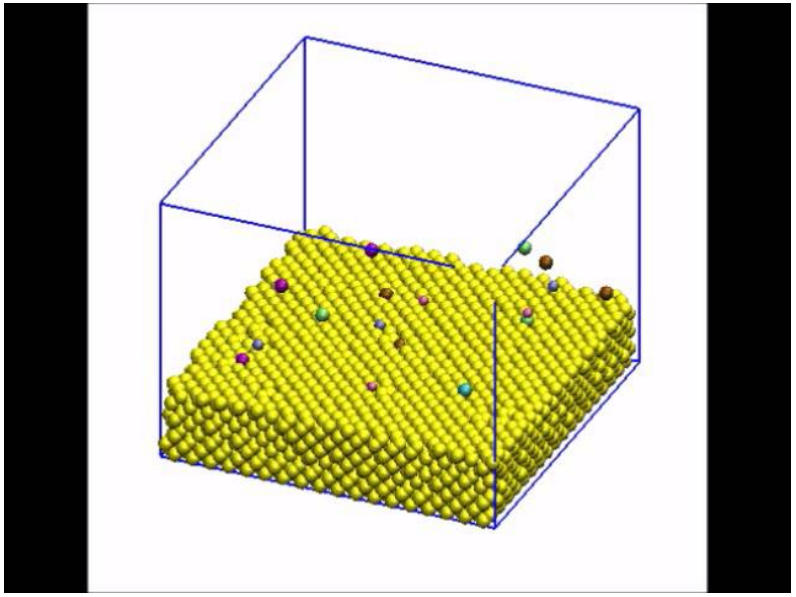

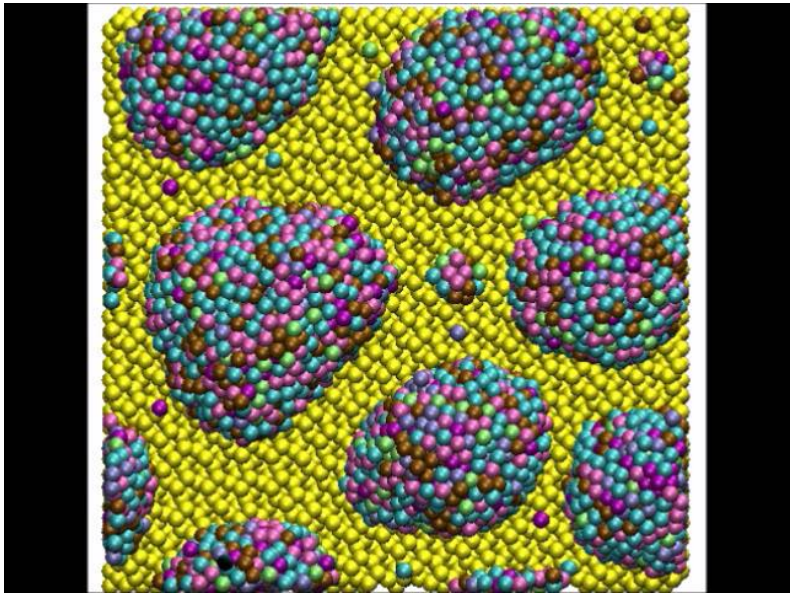

HEA : AlCoCrCuFeNi
Annealing from 25 to 1200°C

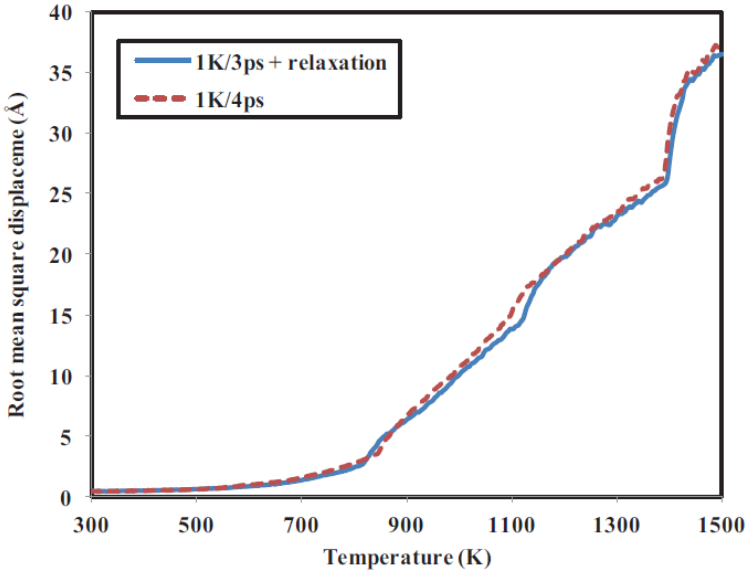

Fig. 4. The comparison of the total root mean square displacement against the temperature between the two annealing methods at the slowest annealing rates.

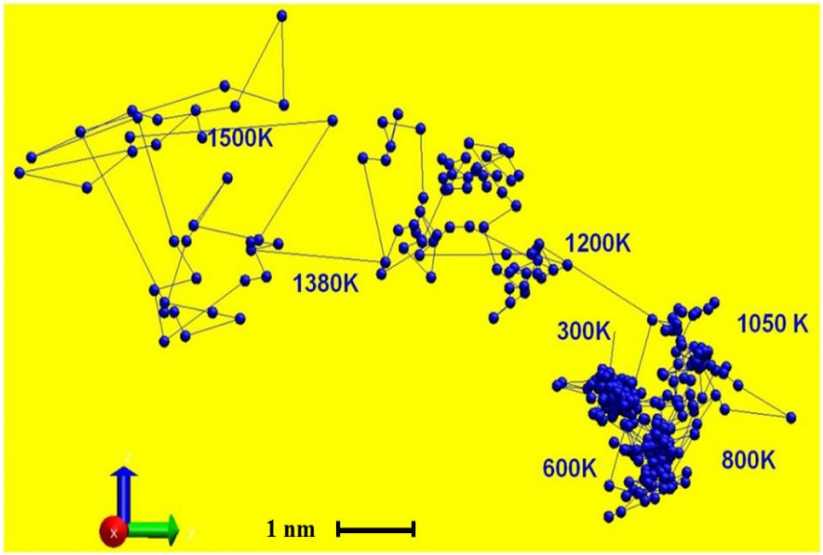

Cluster coalescence/melting around 700°C

Above 700°C, staircase structure of RMSD corresponding to stepwise cluster melting

→ consistent with thermal relaxation time: ps range

→ consistent with experiment (Temperature resolved XRD : 600°C)

HEA : AlCoCrCuFeNi
Temperature Controled XRD

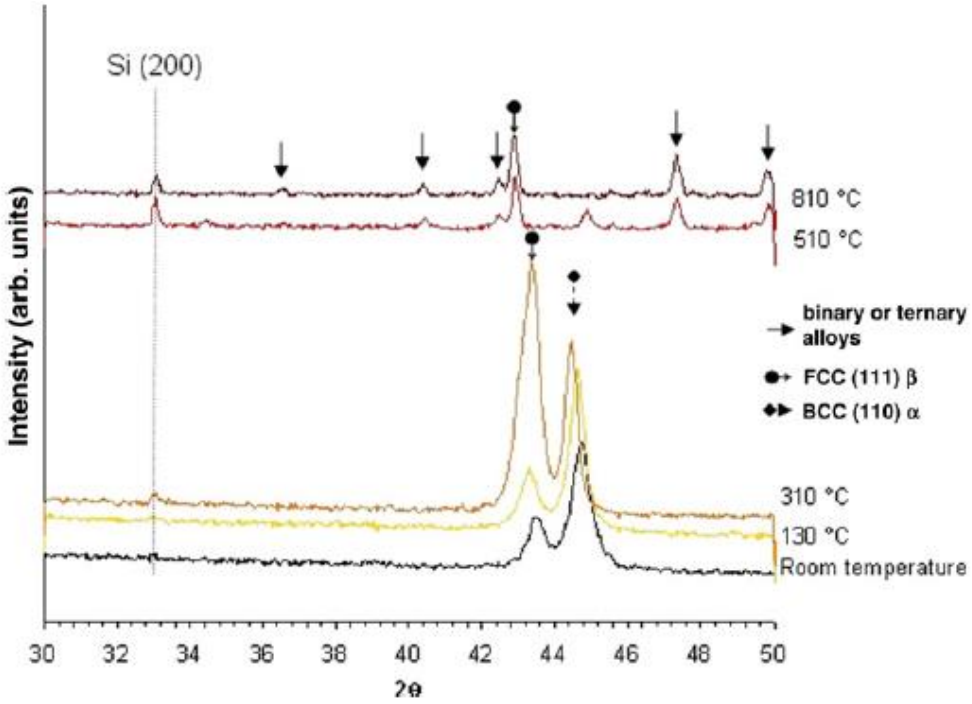

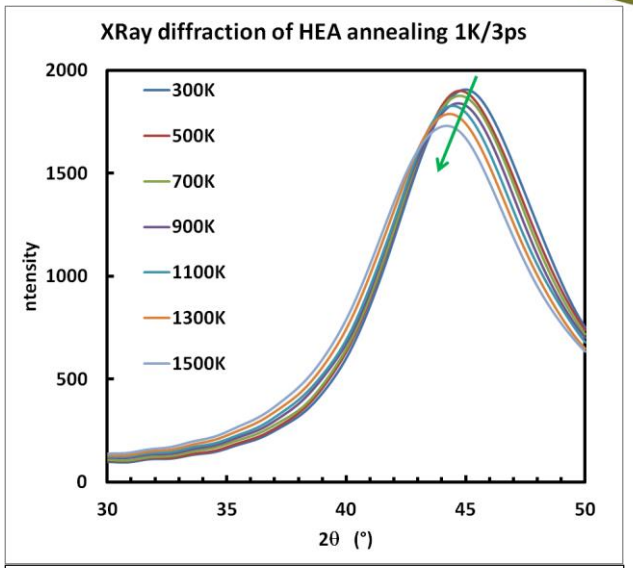

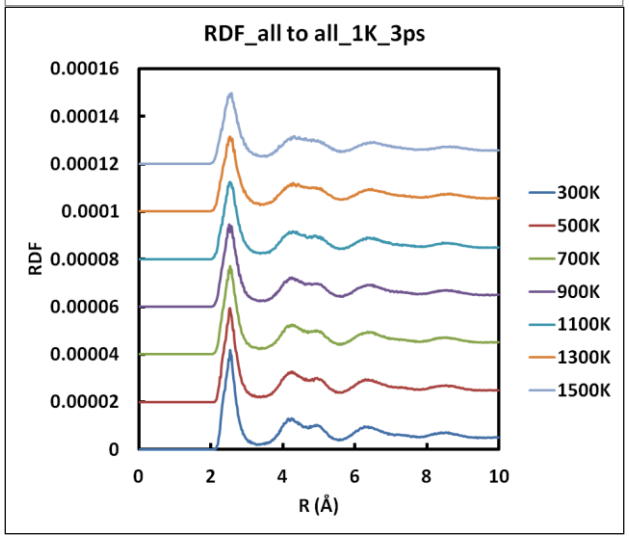

Temperature XRD

V. Dolique et al, Surface & Coatings Technology 204 (2010) 1989–1992

Comparison between Experiments and Simulations

Transition bcc → fcc when T° increases

No crystallisation

$Mg_xAl_yO_z$ thin films grown on a MgO (100)

$$V_{ij} = \frac{q_i q_j}{4\pi\varepsilon_0 r_{ij}} + A\exp\left(-\frac{r_{ij}}{\rho}\right) - \frac{C}{r_{ij}^6}$$

Two potential sets with full (FC) and partial (PC) charges

	i–j	A (eV)	ρ (Å)	C (Å^6 eV)
FC	Mg^{2+}–O^{2-}	1279.69	0.29969	0.0
	Al^{3+}–O^{2-}	1374.79	0.3013	0.0
	O^{2-}–O^{2-}	9547.96	0.21916	32.0
PC	$Mg^{0.945+}$–$O^{0.945-}$	32 586	0.178	27.32
	$Al^{1.4175+}$–$O^{0.945-}$	28 480	0.172	34.63
	$O^{0.945-}$–$O^{0.945-}$	6463.4	0.276	85.22
	$Mg^{0.945+}$–$Mg^{0.945+}$	17 650 254	0.080	8.76
	$Mg^{0.945+}$–$Al^{1.4175+}$	22 981 293	0.074	11.10
	$Al^{1.4175+}$–$Al^{1.4175+}$	31 574 470	0.068	14.07

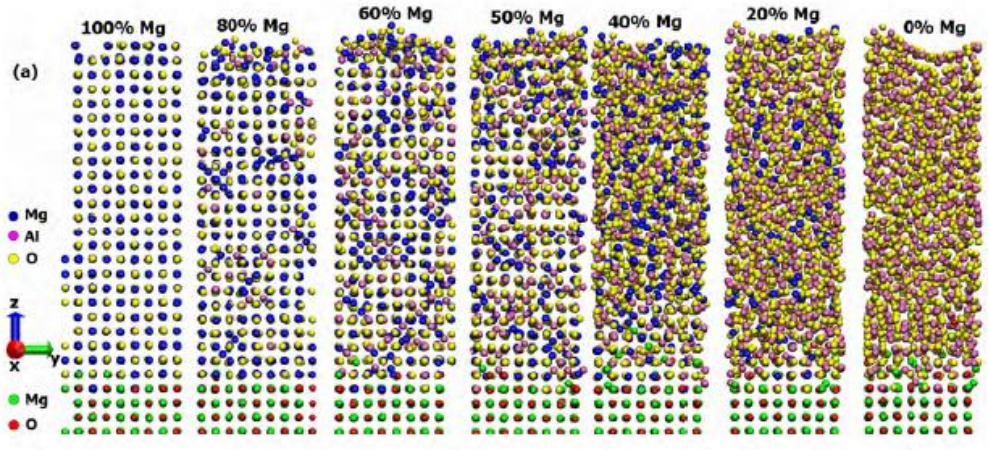

Snapshots of $Mg_xAl_yO_z$ thin films using FC potential: compared successfully to sputtering exp.

V Georgieva, M Saraiva, N Jehanathan, O I Lebelev, D Depla and A Bogaerts, Sputter-deposited Mg–Al–O thin films: linking molecular dynamics simulations to experiments, J. Phys. D: Appl. Phys. 42 (2009) 065107

❑ Conclusion

MD is appropriate for inght into basic mechanisms of sputtering and deposition, provided close connection and comparison to experiments are met
Especially initial conditions and energy treatment during interactions.

❑ Challenging perspectives

Investigation of the reactive sputtering processes at the molecular scale
Complex oxide materials deposition: beyond pair potentials
Complex substrates (porous, …)
Coupling MDS of sputtering and deposition to reactor models
Suitable potential (ReaxFF, COMB, REBO, …)

Many thanks for your attention